NUMERICAL MODELING AND PARAMETRIC STUDY OF LASER ABLATION FOR FABRICATION IN MICROFLUIDICS

A Thesis Presented

By

Matthew James Benton

Presented to the Jackson College of Graduate Studies of the University of Central Oklahoma in Partial Fulfillment of the requirements for the Degree of

MASTER OF SCIENCE IN ENGINEERING PHYSICS – ELECTRICAL ENGINEERING

April 2018

i

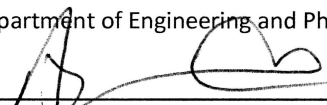# Numerical Modeling and Parametric Study of Laser Ablation for Fabrication in Microfluidics

A THESIS

APPROVED FOR THE DEPARTMENT OF
ENGINEERING & PHYSICS

By _____   4/19/2018

Dr. Mohammad Hossan   Date
Committee Chairperson
Department of Engineering and Physics

_____   4/19/18

Dr. Evan Lemley   Date
Committee Member
Department of Engineering and Physics

_____   04-19-2018

Dr. Abdellah Ait Moussa   Date
Committee Member
Department of Engineering and Physics

ABSTRACT

NUMERICAL MODELING AND PARAMETRIC STUDY OF LASER ABLATION FOR FABRICATION IN MICROFLUIDICS

April 2018

Matthew James Benton

University of Central Oklahoma

Directed by: Dr. Mohammad Hossan

Abstract

Use of CO_2 lasers in the micro-fabrication processes has emerged as a promising technique for mass production of microfluidic devices. Laser micromachining offers competitive advantages over photolithographic processes including better precision, automation, faster production rate, and repeatability. However, optimization of process parameters for smoother channel surface and better control of uniform channel depth is still a challenge, which hinder its wide spread application in micro/nano fabrication of microfluidic devices.

This thesis project studied the impact of laser system parameters and thermo-physical properties on the laser micromachining of microchannels through mathematical modeling. Three and two-dimensional transient heat conduction equations with laser heat generation were solved using finite element based Multiphysics software COMSOL. Laser heating source profile is considered

to follow Gaussian distribution. Grid independent analysis was performed for ensuring accuracy of the model, and the equivalency of three and two-dimensional model was also verified.

The developed model was used to investigate laser fabrication in two main ways. The first was by looking at the effect of laser spot size, scanning speed, and power on the resulting channel width, depth, and shape. The second was to conduct a parametric study of the effect of the various relevant thermal properties on the resulting cut geometry. Channel depth was measured from the simulation using a cut off temperature of 700K. The results show that the laser power and scanning speed has strong effect on the channel depth, whereas the laser spot size effects both depth and width of the channel. The higher thermal conductivity of a material has deeper cut for the same laser system parameters. The results also show that the channel depth can be varied by facilitating higher convective heat transfer coefficient. The temperature dependent specific heat in the model results in different channel depth compared to the constant specific heat model. This study can help in optimizing process parameters and better understand the effect of thermo-physical properties of microdevice substrates in laser micromachining. Thus, it will contribute to solving current challenges in laser micro-fabrication processes.

Acknowledgements

Table of Contents

List of Tables and Figures

Chapter 1: Introduction

1.1. Background

Microfluidics have been shown to have a broad range of potential applications in chemistry, biology, and engineering. Methods for miniaturizing numerous lab techniques have been found and implemented in microfluidics devices. In many cases, these devices offer several advantages over using more traditional equipment. They are often less expensive to produce, require smaller sample volumes, and require less reagents which further reduces costs. Microfluidics devices can also offer much greater portability, as well as faster processing and analysis [1]. Despite all the potential advantages, the use of microfluidics remains limited.

Fabrication of these devices is an ongoing challenge, with many existing techniques each with their own limitations. Chemical etching and photolithography were among the first techniques used, which were borrowed from the established microelectronic industry. These methods are expensive due to both material and set up costs, because they were mainly limited to glass and other silica based materials. Additionally, these materials are incompatible with many chemical and biological applications [2]. Soft lithography is a much cheaper and quicker alternative, which is very useful for prototyping, though it is mainly limited to use with PDMS [2]. Hot embossing and Injection molding methods have been developed for more efficient, larger scale manufacturing with a wider range of materials. However, these methods require a mold that must be fabricated using other methods beforehand, making them inefficient for prototyping and small-scale production [3, 4, 5].

One method that has recently shown promise in overcoming many of the issues is laser ablation. Laser ablation utilizes an intensely focused beam to either photochemically or photothermally break down a material. There are two main types of laser ablation, using either pulsed ultraviolet (UV), or continuous infrared (IR) lasers. Pulsed laser ablation has been found to provide for quick fabrication, though complexity and cost have limited its use in practice [6, 7]. On the other hand, continuous laser ablation, mainly in the form of CO_2 lasers, has shown to be both quick and cheaper. However, the extent of its use in literature has been quite limited. More research is necessary in order to better establish the use of lasers in microfluidic fabrication. A more complete understanding of how laser system parameters and material choice influence the removal of material is a necessary step towards this goal.

1.2. Thesis Statement and Objectives:

The work presented here has two main components. First, a three-dimensional computational model is developed to investigate the thermal-based material removal in polymers subjected to a continuous, focused laser beam. The effect of laser spot size, laser scanning speed, and laser power on the resulting channel width, depth, and shape are investigated. Second, a two-dimensional model is developed to conduct a parametric study of the effect of various relevant thermal material and system properties on the resulting cut geometry. Thermal conductivity and specific heat of materials are considered, as well as the convection coefficient corresponding to the process. The goal of this work is to understand the effect of both laser parameters and thermo-physical properties of the substrate materials on the channel depth and shape in CO_2 laser fabrication of microfluidic devices. Investigating the effect of laser system parameters and key thermal properties in laser cutting will serve as a tool to help determine the effectiveness of

2

laser fabrication on different potential materials. A summary of these objectives is provided below:

1. Develop 3D and 2D models of laser ablation for fabricating microfluidic channels using COMSOL Multiphysics

2. Investigate the effect of laser system parameters on resulting microfluidic channel. Parameters include laser spot size, scanning speed, and power.

3. Investigate the effect of thermo physical properties on resulting microfluidic channel. Parameters include convection coefficient, thermal conductivity and specific heat of the material.

1.3. Organization of Thesis

The thesis is organized as follows: Chapter 2 contains a literature review which gives an overview of fabrication in microfluidics and covering existing literature on CO_2 laser ablation. Chapter 3 provides a theoretical description of laser ablation, and describes the model used in this thesis. Chapter 4 contains the results and discussion. Chapter 5 summarizes the results, concludes the thesis, and provides suggestions for future studies.

Chapter 2: Literature Review

2.1.   Introduction

In recent years, the use of microfluidics has become an area of intense research. This is motivated by a need for more compact, versatile tools and analytical methods for various applications in chemistry, biochemistry, and molecular biology [8]. As a result, microfluidic systems have been investigated and developed for numerous biological and chemical techniques. These applications include methods of capillary electrophoresis [9, 10, 11, 12], flow cytometry [13, 14], polymerase chain reaction (PCR) [15, 16, 17], and protein analysis [12, 18, 19]. In addition, researches have demonstrated the capability of performing various other procedures that would be necessary in a wide range of application. These applications include sample mixing [20, 21, 6], separations [22, 23], treatments, and chemical reactions [20, 24], among many others.

Many of these processes can be run in parallel or integrated into a single device to provide a so-called lab-on-a-chip (LOC) to perform specific laboratory tasks. These LOC devices provide several advantages over traditional methods depending on the application. The advantages of LOC devices include reduced sample volumes and reagent costs, faster analysis and processing, and greater portability [8]. Two of the most important factors in the application of these devices are the choices of material and fabrication methods. Silica based materials, such as glass, are commonly used, though recently polymer materials, such as PDMS and PMMA, have gained significant attention in research. For each of these materials, several fabrication techniques have been developed and have continued to be improved in recent years, though much more research in the area is still needed.

2.2. Materials used in Microfluidics

Many earlier microfluidic devices were made using glass and silicon. The use of these materials was mostly due to convenience, with fabrication methods already developed for these materials for use in microelectronics and microelectromechanical systems (MEMS). Additionally, glass was preferred due to its high compatibility with electrophoretic phenomena, which are the driving forces in many microfluidic systems [25]. However, these materials are often inappropriate for various chemical and especially biological analyses. Silicon for example is expensive, and opaque to both UV and visible light which renders conventional optical detection methods impossible [2].

Due to the limitations on glass and silicon based materials, most recent attention in research in microfluidics has focused on the use of polymers, such as polydimethylsiloxane (PDMS). PDMS is an elastomer that is one of the most widely used polymers for microfluidic systems due to several favorable properties. This includes low cost and availability, transparency to visible through near ultraviolet (UV) light, flexibility, and chemical inertness [2]. Another big factor in the use of PDMS was the development of soft lithography fabrication technique for faster prototyping [26]. This, along with the low cost and availability, allow for much cheaper prototyping than glass. This in turn allows for new designs and improvements to be made quickly and easily. However, the use of PDMS is not without its own drawbacks. One significant issue is absorption. PDMS is known to absorb small hydrophobic molecules and hydrocarbon solvents, which can limit the potential number of applications [27]. PDMS is also vapor permeable, which can allow for unwanted evaporation [28] to occur through PDMS. Additionally, the hydrophobic nature of PDMS can

present concerns. Researchers have used surface modification in attempts to avoid the issues of hydrophobicity [29, 30], although these modifications also complicate the fabrication process.

It is clear that other materials are necessary in many cases where PDMS is not adequate. For this, researchers have turned their attention towards various other polymers. One that has gained much of this attention is poly(methyl methacrylate), or PMMA. PMMA is considered a good candidate material for use in microfluidics for several reasons. For one, it is resistant to hydrolysis and chemically inert in aqueous solution. Unlike PDMS, it is also not vapor permeable, since it is a non-porous solid. This eliminates the concern for absorption at the microchannel walls. Various other polymers have also been considered for use in microfluidics, including polycarbonate. polyethylene terephthalate (PET), and polytetrafluoroethylene (PTFE). The use of other polymers however, has been limited relative to PDMS and PMMA. This is likely at least in part due to limited knowledge and availability of fabrication techniques compatible with these other materials. For example, PDMS, despite its shortcomings, is the most widely used material in microfluidics mainly due to easier curing and processing. PDMS as a material for microfluidic devices is well established in the field of microfluidics.

2.3. Common Fabrication Methods

Though the choice of material is an important aspect of microfluidics, the fabrication method used is inextricably linked to that choice. Several fabrication techniques have been developed to use with different materials. Photolithography and chemical etching were among the first fabrication methods used in microfluidics. Borrowed from the microelectronics industry, these techniques are used to fabricate microfluidics devices in silicon and glass. These methods are expensive and inaccessible for many researchers especially in low-resourced areas, limiting their

development and use in application. A solution to this issue came in the form of a method called soft lithography used to fabricate devices with PDMS.

Soft lithography borrows from photolithography techniques developed for the microelectronics industry. The process is shown in figure 2.1. First, a negative photomask of the channel design is printed. Then, a photoresist is spin coated onto glass and exposed to UV light through the photomask. Photoresist developer is then
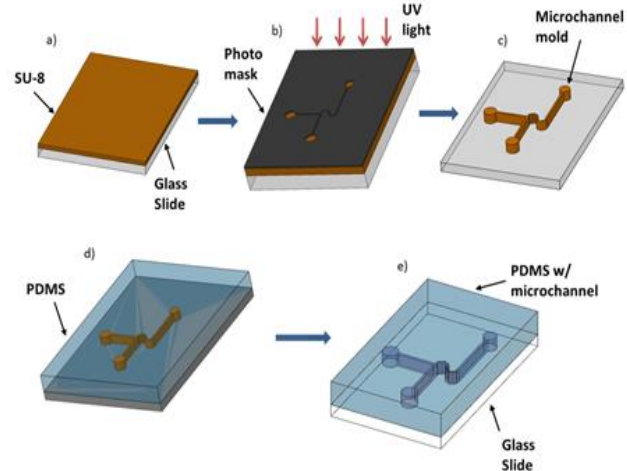
Figure 2.1: Soft Lithography Process for Microfluidic Fabrication of PDMS

used to remove excess, unexposed developer, leaving a positive copy of the channel on the glass surface. The positive mold can then be used to create replicas of the microchannel by molding [31]. The use of soft lithography has allowed researchers to create and test new designs in short time frames, typically less than a couple days from design to experiment ready device.

Although soft lithography allows for quicker prototyping on PDMS, other fabrication methods, including hot embossing and injection molding, have been developed and investigated for cheaper, more efficient manufacturing of microfluidic devices in larger volumes. Hot embossing has been used to create microfluidic systems in polycarbonate and PMMA. First, an embossing master is created using photolithography or other methods on silicon or various metals [32]. Then, this master is used to imprint the device design onto a substrate. The process takes between 5-15 minutes depending on the system and material used [5]. In injection molding, a metallic mold inside a cavity, where a thermoplastic material is heated past its melting

7

temperature, injected, and held under pressure to form fit the mold until it cools below its glass transition temperature and solidifies. This process can be fully automated with very short cycle times, between a few seconds to a few minutes depending on the material [4].

Though soft lithography is an effective fabrication technique for prototyping, it is only effective for use with elastomers, mainly PDMS. Other polymer materials with potential application in microfluidics, such as polycarbonate and PMMA, require different fabrication techniques. Though the replication techniques presented can be successfully applied to many other polymers, they lack the flexibility required for prototyping. One method that has shown promise in this regard is laser ablation.

2.4. Use of Lasers in Fabrication

Industrial lasers can be found in use by countless industries. From material treatment, to cutting, to welding, the laser is one of the most versatile tool available for manufacturing and material processing. In many processes, lasers provide distinct advantages over traditional fabrication techniques. These advantages often include improved processing speed and quality, which directly increase productivity. The flexibility of lasers in general also allows for innovation by enabling novel manufacturing and design. In many cases, lasers are used to overcome limitations in manufacturing imposed by otherwise traditional fabrication techniques [33].

2.5. Laser Fabrication in Microfluidics

Recently, researchers have been working towards expanding the use of lasers into the realm of microfluidics. The use of lasers in microfluidics up to this point can be broken down based on the type of laser used. There are two main types of lasers used, either pulsed UV light lasers, or

continuous infrared (IR) light lasers. UV lasers use high energy light to induce highly targeted breakdown of materials in very short pulses. This type of laser has been used to add un-moldable features to generic microchannels produced by typical mold-based techniques for custom functionality [7, 6]. UV lasers have also been used to directly machine microchannels in PMMA [34, 35]. Though this method provides quick fabrication for prototyping and allows for a potentially broader range of applications, low repetition rate and cost generally limit its use [36].

Meanwhile, the use of IR laser processing has also been considered and shows great promise. IR laser systems, mainly in the form of CO_2 lasers, are commercially available at moderate prices and already in widespread use in industrial applications [37]. As a result, IR laser ablation has significant potential for fast, flexible, and low-cost prototyping of polymer microfluidic systems. Klank et al. [38] first demonstrated the use of an
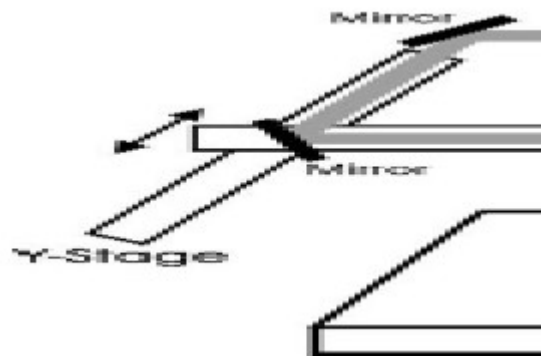
Figure 2.2: Configuration of a typical laser machining stage. Adopted from Cheng et. al. [39]

industrial CO_2 laser as an effective alternative to UV laser systems for fabricating microfluidic devices in polymer materials. The study focuses on PMMA, which can be compared to other existing micromachining techniques. Additionally, the products of thermal decomposition of the polymer material used is an important consideration, as the mechanism for material removal is purely thermal in the case of CO_2 lasers. PMMA decomposes into volatile products, leaving clean structures behind. However, there were some concerns that were soon discovered. The first concern was the presence of a bulge around the rim of the channel, likely due to resolidification

of ejected material. Also, the roughness of the fabricated microchannels were found to be on the order of 1-10um, which can limit use in application [38].
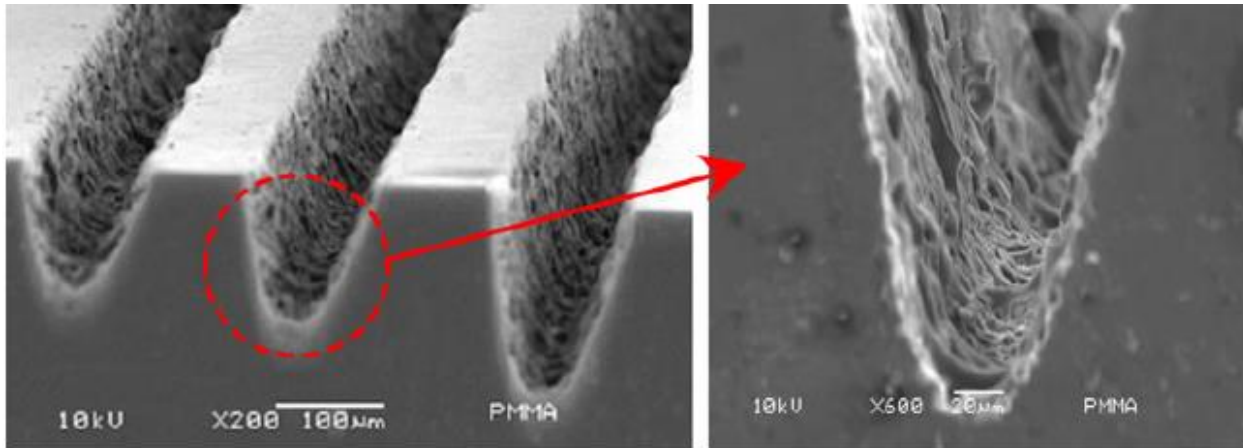
Figure 2.3: Roughness on as-machined PMMA. SEM images of machined PMMA showing the roughness that occurs. Adopted from Hong et. al. [13]

Cheng et. al. [39] further investigated the use of CO_2 laser ablation, considering the use of thermal annealing to overcome the problem of surface roughness. It was found that by applying a simple thermal annealing process, roughness can be brought from 1-10um in as-machined PMMA down to around 2-3nm. They also found that by controlling laser system parameters, such as the scanning speed, laser power, and number of passes, aspect ratios of 0.5-7+ could be achieved on a single PMMA substrate. In addition to the roughness problem, the bulging distortion at the channel rim was also investigated. The authors found that there are two types of PMMA available commercially, extruded and cast, and that the type influences the distortion. It was found that while extruded PMMA had reduced roughness, the bulges were more present. Cast PMMA meanwhile showed more roughness, but negligible rim distortion [39]. Another approach to address the roughness concern, proposed by Hong et al. [13], uses an unfocused CO_2 laser beam for fabrication. It was found that aspect ratios could be similarly controlled through varying laser

parameters, with a roughness of less than 4nm, avoiding the need for additional post processing

such as annealing.

Figure 2.4: Rim bulging on machined PMMA. SEM images of machined PMMA. Adopted from Cheng et. al. [39]. a.) Cast PMMA without annealing. b.) Cast PMMA after annealing. c.) Extruded PMMA without annealing.

Various groups have used CO_2 laser ablation to fabricate channels in application in PMMA, as well

as other polymer materials. Liu et. al. [15] used a CO_2 laser set up to create disposable integrated

devices for genetic assay in polycarbonate. The device successfully integrated PCR amplification,

DNA hybridization, and hybridization wash functions. Wang et al. [40] created a microfluidic

device in Vivak co-polymer capable of producing electroosmotic flow and electrophoretic

separations without complicated surface modification otherwise required in PMMA devices to
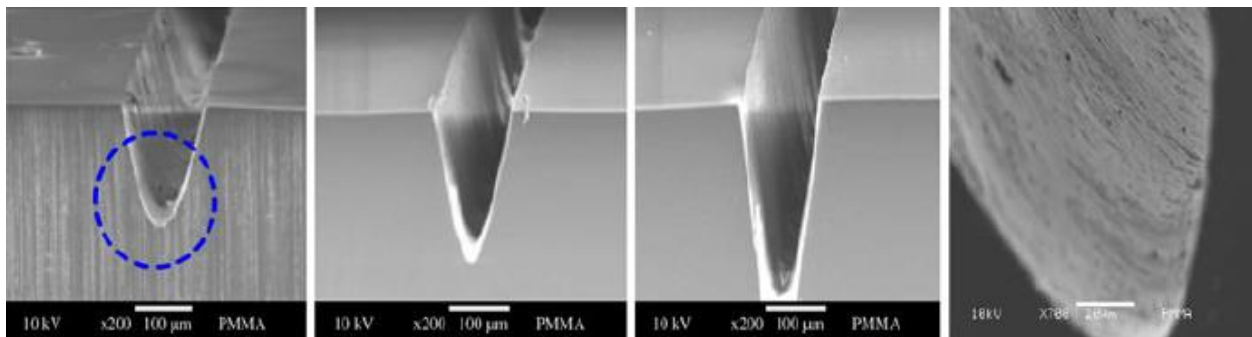
Figure 2.5: Roughness of machined PMMA using unfocused laser beam technique, developed by Hong et al. [13]. Figure also adopted from Hong et. al.

achieve similar results. Yang et al. [41] used a CO_2 laser on PMMA to create a device for creating

chitosan microparticles encapsulating ampicillin with high throughput and size-controlling

capabilities. Hong et al. [13] created an integrated rapid methanol detection system, as well as a

11

flow cytometer.   Hou et al. [42] fabricated a 3D microfluidic device for rapid glucose detection using CO_2 laser on PMMA.

2.6.   Current State of Modeling Microfluidic Laser Fabrication

Despite the interest in application of CO_2 laser ablation, there is not as much existing literature on numerical modelling and simulation of the process. In many applications, a high degree of precision and accuracy is needed in fabrication to successfully implement and integrate various processes in a microfluidic system. To design, and especially optimize, designs for application, the fabrication method must be very well controlled and understood. In the case of CO_2 laser ablation, laser speed, spot size, and intensity, as well as the optical and thermal properties of the substrate all have a significant effect on the resulting structures. Being able to predict and understand how each of these parameters affect the resulting fabricated structures is necessary to better inform researchers on how to design and create systems using CO_2 laser ablation.

As mentioned previously, several groups have experimentally investigated laser system parameters for fabrication in PMMA. Some groups have also developed theoretical and numerical models of these parameters as well. Snakenborg et al. [37] first created a simple model for estimating the depth of a channel cut by a CO_2 laser in PMMA. The model assumes that all heat is absorbed at the surface, and that the amount of material removed is proportional to the amount of heat added. By calculating the amount of heat required to remove material, as well as the heat required to raise the material temperature from room temperature to the vaporization temperature. One noted limitation is that the model assumes that the heat is confined within the directly irradiated region, with no conduction occurring. Additionally, it does not consider the temperature dependence of the various physical properties within the model.

12

Tresansky et. al. [43] used COMSOL multiphysics modeling software to create a computational heat transfer model of CO_2 laser ablation. They created a 2D axisymmetric model of polymer to simulate the removal of material using a CO_2 laser during drilling. In this model, the researchers developed a relatively simple method of approximating the
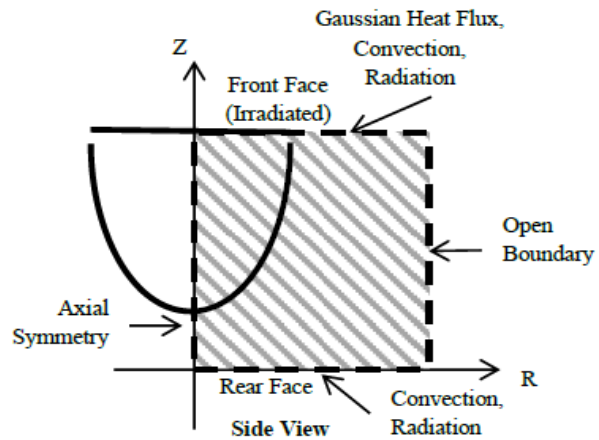
Figure 2.6: Diagram of numerical model used by Tresansky et. al. [43].

phase change and material removal that occurs during laser ablation. By introducing step changes in the thermal properties at the vaporization temperature, the model treats the material at that temperature as if it were removed, without requiring numerically intensive element removal and re-meshing at each step. Using this method, the drilling of PMMA and a carbon fiber reinforced polymer composite, for depths up to 6mm.

Despite the handful of reports on the modelling of CO_2 laser fabrication described above, there is a need for comprehensive studies to understand the underlying physics in laser micromachining and the effect of laser parameters and material properties on channel depth, shape, and roughness. In addition, an optimization of protocols combining laser parameters and substrate thermo physical properties is needed for rapid mass production of microchannels and devices. The work presented in this thesis provides a much-needed comprehensive look at both physical and laser properties to increase understanding of how those parameters impact the resulting channels to be fabricated. This knowledge will allow for much more informed decisions to be made in terms of material choice and microchannel design.

Chapter 3: Theory and Model Formulation

3.1. Background Theory

The breakdown of materials using lasers can generally be described as photochemical or photothermal in nature. Photochemical ablation by lasers occurs by the absorption of photons that cause a direct breakdown in chemical bonds. In photothermal absorption, the energy is absorbed as heat, rapidly increasing the temperature of the material in the irradiated region. The material first melts and then decomposes due to the heat, leaving a void. In the case of ultraviolet (UV) lasers, the mechanism is often a complex combination of the two. However, with infrared (IR) lasers, such as the CO_2 laser (10.6um), the mechanism is purely photothermal. Therefore, in the case of CO_2 lasers, the ablation process can be modeled as a purely thermal event.

When a continuous laser beam is moved across the surface of a polymer, a portion of the material is vaporized, while another portion is melted into a liquid form. This occurs at the spot where the laser meets the surface. The vaporized material expands and escapes, which drives the liquid polymer outward along with it. In this way, some of the liquid material is ejected, while the rest remains in the channel and re-solidifies in the wake of the beam. By moving the laser across the surface, a channel and other similar structures can be cut into the material. The cross section of the resulting channel depends heavily on the material, namely the thermal diffusivity and the mechanisms of thermal decomposition for the specific polymer.

Although the material undergoes phase change as it is heated by the laser, most of the heating process occurs in the solid phase. Once the material reaches the point of phase change, it quickly changes phase and is removed from the bulk solid material. To avoid over-complications in the

14

model, we focus our attention on the solid material, while treating the phase change and subsequent material removal as a convection boundary condition, which will be described in further detail later in the section.

3.2. Governing equations:

3.2.1. Heat Equation:

To model laser cutting as a thermal event, the heat equation for a solid material is used:

$$\rho C_p \frac{\partial T}{\partial t} = -\nabla \cdot (k\nabla T) + \dot{q}_V \tag{3.1}$$

Where ρ is the density, C_p is the constant pressure specific heat, and k is the thermal conductivity of the material. The $\dot{q}_V$ term represents volumetric heat generation. This partial differential equation is solved for the temperature distribution in space and time.

3.2.2. Laser Heating:

The heat from the laser beam is introduced by absorption starting at the surface. The absorption is modeled following Beer's Law, giving the following expression for the specific power density [44]:

$$P_d(r, z) = \alpha I(r, z)e^{-\alpha z} \tag{3.2}$$

Where α is the material's absorption coefficient (m^{-1}) and $I(r,z)$ is the intensity of the laser at a distance r from axis of the beam, the z-coordinate is the distance from the surface of the substrate measured downwards in the direction of the beam.
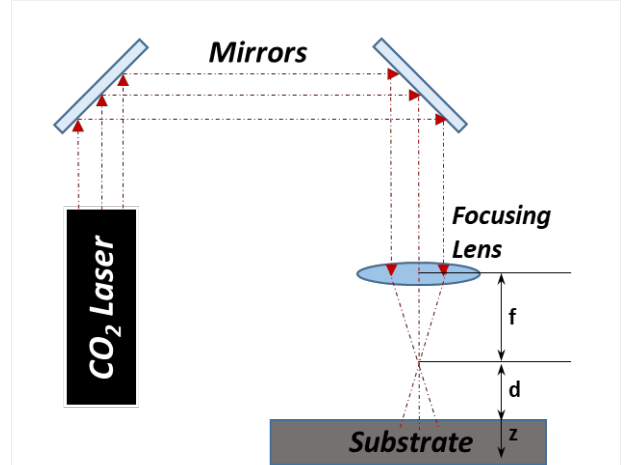
Figure 3.1: Schematic of modeled laser set up.

The intensity of most laser beams can be treated as a gaussian beam, whose intensity profile is given by a gaussian function:

$$I(r, z) = I(0, z)e^{-\frac{2r^2}{w(z+d)^2}} \qquad (3.3)$$

Where $I(0,z)$ is the peak intensity along the beam axis, $w(z)$ is the beam radius, or spot size, at which point the beam intensity falls to $1/e^2$ of its value along the beam axis, and d is the distance from the substrate to the beam waist, where the beam radius is minimum.

The size of the beam, described by the beam radius, is given by the following function [45]:

$$w(z) = w_0\sqrt{1 + \left(\frac{\lambda z}{\pi w_0^2}\right)^2} \qquad (3.4)$$

Where λ is the wavelength of the laser and w_0 is the waist radius, the minimum radius of the laser beam.

The peak intensity, $I(0,z)$ can be given by:

$$I(0, z) = \frac{2P_0}{\pi w(z+d)^2} \qquad (3.5)$$

16

Where P_0 is the total power of the laser beam.

Assuming the beam radius is approximately constant over relevant z values, the beam radius becomes a constant w_0. Combining and simplifying equations (2)-(5), and using $r^2=x^2+y^2$,

$$P_d(x,y,z)=\frac{2P_0\alpha}{\pi w_0^2}e^{-\frac{2(x^2+y^2)}{w_0^2}-\alpha z}$$
(3.6)

For laser cutting, the laser beam is moved continuously across the surface. Assuming the laser beam moves at a constant velocity, $_L y$ along the x-coordinate direction, the time dependent power density can be written as:

$$P_d(x, y, z, t) = \frac{2P_0\alpha}{\pi w_0^2}e^{-\frac{2[(x-V_Lt)^2+y^2]}{w_0^2}-\alpha z}$$
(3.7)

3.3.   Formulation of Model in COMSOL

To create a numerical model of the problem and solve it, a finite element based commercial multiphysics software, COMSOL Multiphysics 5.2a software is used.

3.3.1. Three-dimensional model

First, a 3D model of the material is created within COMSOL. The x and y-dimensions are parametrically defined based on the size of the laser beam and channel length, to ensure that
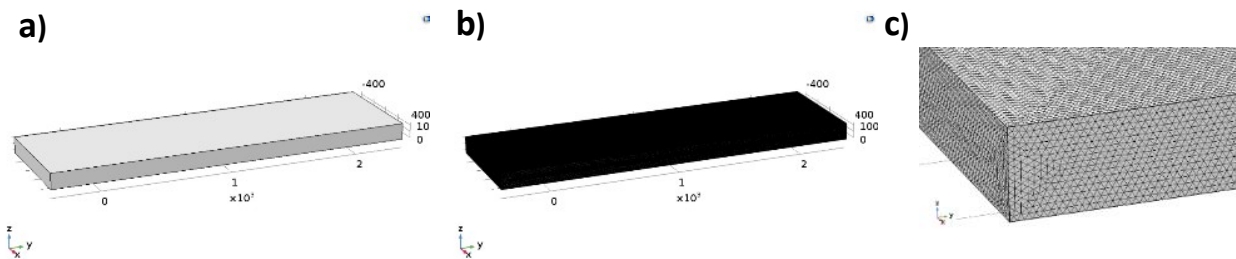
Figure 3.2: Three-dimensional model geometry and meshing. Dimensions are given in um. a) 3D Model geometry. b) Meshed 3D geometry (10um maximum element size). c) Zoomed-in image of 3D meshing

the region affected by heat is entirely contained within the model. The geometry of the model is shown in figure 3.2, along with the mesh used.

3.3.2. Two-dimension model

For the 2D model, the plane is taken to be the vertical cross-section down the center of 3D model. The cross section is taken along the axis of the laser motion, so that the laser is centered along the top edge of the 2D model as it moves. This is done so that the depth in the 2D model is the same as the maximum depth in the 3D model. This allows smaller, more accurate meshes to be used, and for parametric studies to be completed more efficiently.
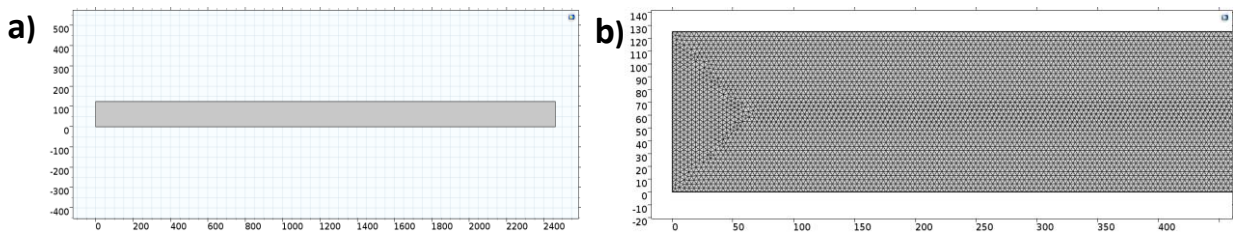
Figure 3.3: Two-dimensional model geometry and meshing. Dimensions are given in um. a) 2D Model geometry. b) Meshed 2D geometry (4um maximum element size)

3.3.3. Model Formulation

The time dependent heat equation, equation (1), is solved for the domain shown, to find the temperature distribution within the region heated by the laser. The equation is solved within COMSOL using the PARDISO direct solver, with backwards differentiation formula (BDF) time stepping method. These methods were chosen by default through COMSOL for relative speed and accuracy in solving the heat conduction equation. The temperature distribution is then used to determine where material is removed. Material is assumed to be removed once the material reaches the temperature at which phase change from solid to vapor is complete. Although the phase change and material removal for a polymer such as PMMA will occur over a range of temperatures, the heating is assumed to happen rapidly enough that it can be approximated as

18

a step change between solid and vapor phases. As a note, this occurs at T=700K for PMMA [43], although this temperature will change from one material to another. For the purposes of this research, the same value of 700K is used throughout the parametric study, to allow for clear comparison between cases.

The heat transfer due to the laser beam is introduced as a volumetric heat generation term across the entire domain, given by the power density of the laser beam, assuming the focal waist occurs at the top surface:

$$\dot{q}_V = \frac{2P_0\alpha}{\pi w_0^2} e^{-\frac{2[(x-V_L t)^2 + y^2]}{w_0^2} - \alpha z} \tag{3.8}$$

For the material properties, isotropic and temperature independence are assumed, unless stated otherwise.

3.4.   Boundary Conditions

3.4.1. Side walls

In both the 2D and 3D model, all side boundaries are treated as insulating boundaries:

$$k\nabla T \cdot \hat{n} = 0 \tag{3.9}$$

Where $\hat{n}$ is the unit normal vector at the boundary. The material is assumed to extend in all directions beyond the given model. In thermal modeling, a heat-affected zone (HAZ) is a region of material in which material undergoing heating has not been melted, but is still affected by an increased temperature from the base material. It is assumed that the entire HAZ is contained within the given model.

3.4.2. Top surface

On the top surface, a combination of radiation and convection heat transfer occur:

$$-k\nabla T \cdot \hat{n} = h_c(T_\infty - T) + \varepsilon\sigma(T_\infty^4 - T^4) \qquad (3.10)$$

Where h_c is the convective heat transfer coefficient, ε is the emissivity of the material, and σ is the Stefan-Boltzmann constant. The value for the convective heat transfer is generally calculated using one of many of empirical relations corresponding the situation of interest. The choice of convection coefficient is described in detail in the next section.

3.4.3. Convection Coefficient Consideration

In most models involving heat convection, the convection coefficient is found using experimental correlations established for a given flow situation. For the case of laser ablation, determining an applicable correlation is exceedingly difficult. Until the material reaches the temperatures at which melting occurs, the flow situation would best be described as natural convection over a horizontal plate, which yields very low convection coefficients, on the order of 10 W/m ^{2}K [38]. Once the temperature reaches the melting temperature, and then especially the vaporization temperature, the situation becomes complex. When first melting, heat convection occurs at the solid-liquid boundary, as well as between the liquid and the surrounding air. Once the liquid begins to vaporize, the vapor boils out of the liquid, quickly expands, and escapes, removing large amounts of heat energy with it due to convection. Additionally, in the case of laser ablation, these processes occur rapidly, further complicating the matter.

Since no existing literature seems to have investigated this in any detail, this study explores the use of convection coefficient as a method for modelling phase change and the heat loss

associated with this. For this, a wide range of values are considered. The lower end of values

considered (250 $Wm^{-1}K^{-1}$) generally correspond to forced convection with fan cooling. The upper

range of convection coefficients is chosen to be on the same order as heat transfer coefficients

(~$1x10^5$ $Wm^{-1}K^{-1}$) seen in pool boiling heat transfer, a similar phenomenon where boiling occurs

on solid-liquid interface due to the solid surface temperature exceeding the saturation

temperature of the liquid. A phase transition occurs, forming bubbles that escape, resulting in

very high levels of convective heat transfer [46].

3.5. Mesh Convergence

The mesh used for the simulations in this thesis are generated using COMSOL's physics controlled

meshing preset, which uses second order unstructured tetrahedral elements for 3D and

triangular elements for 2D. The meshing is then controlled by varying the maximum element size

parameter. For the 3D model, this is set to 10um. For the 2D model, a convergence analysis is

conducted in order to determine the optimal size parameter to use. The mesh is considered to

be sufficient when the variation of temperature between successively smaller meshes becomes

small.

Table 3.1: Mesh Convergence Information

	32um	16um	8um	4um	2um	1um
# of Elements	938	3410	12974	49422	330824	1321078
DOF solved for	1715	6497	25301	97549	659059	2636981
RAM usage (GB)	2.25	2.27	2.31	2.5	5.84	12.77
Solve Time (s)	6s	15s	30s	1m38s	10m58s	1h12m16s

The maximum element size parameter is used to define the mesh sizes considered. The parameter defines the longest side length of elements within the mesh. Table 3.1 presents information on the computational complexity and solving time for each of these meshes. For each mesh, the same set of parameters is used, and are described in the following chapter of this thesis.
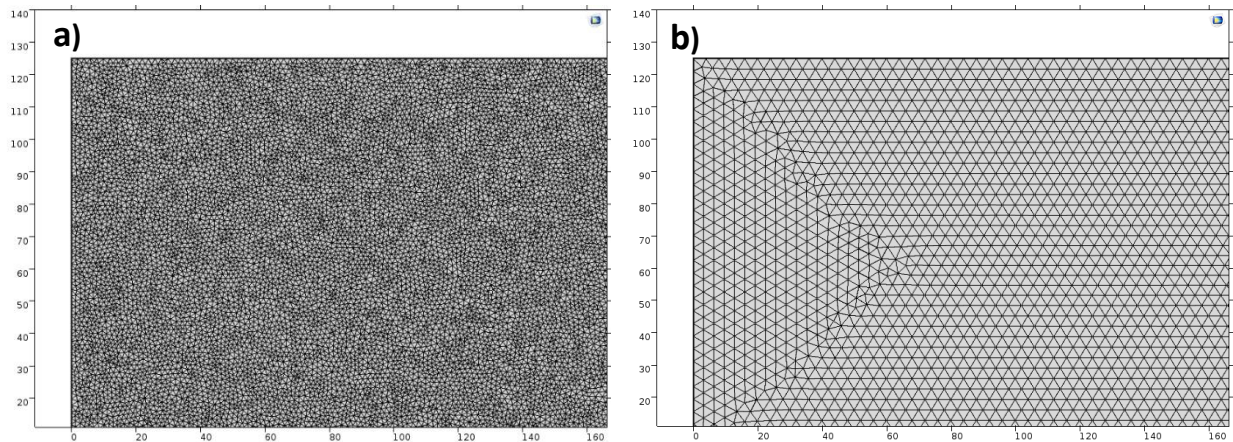
Figure 3.4: Example meshes used during the mesh convergence study. **a)** 4um mesh generated using advancing front method. **b)** 2um mesh generated using Delaunay refinement

The meshes are generated within COMSOL using one of two schemes, either advancing front or Delaunay refinement. The choice is made automatically within COMSOL, depending on which is more applicable. The advancing front produces a more regular pattern with less elements required [47], which can be seen in figure 3.4a. The 32um through 4um meshes utilize this form of refinement. On the other hand, Delaunay refinement shown in figure 3.4b is used for the 2um and 1um meshes. This method produces less structured meshes, although it is more efficient and robust in producing meshes than advancing front [47]. This makes it better for smaller meshes or more complicated geometries, where advancing front does not always converge. This is the case for the smallest two meshes. This change in meshing method explains the significant

increase in computational complexity between the 4um and 2um meshes. It is clear that the 4um mesh or larger would be preferred with regards to computation time.

3.5.1. Direct Temperature Convergence

The first parameter considered for convergence is the temperature distribution. The convergence is considered in two ways. The first is done by determining the percent difference between temperatures at all points in the domain between successively smaller mesh sizes. Second, the depth at which the material reaches 700 K for a given time is considered. This is the point at which material is determined to be removed. Therefore, to select a mesh size, it is most important that the position of T=700K isotherm is converged.

Figure 3.5 contains the results of the mesh convergence on the T=700K isotherm. Figure 3.6 contains the temperature along the depth of the material, at x=1000um. The plots are generated from a grid of preset points generated and evaluated for temperature in COMSOL and exported as a data file for each separate mesh. The points that fall between nodes are automatically
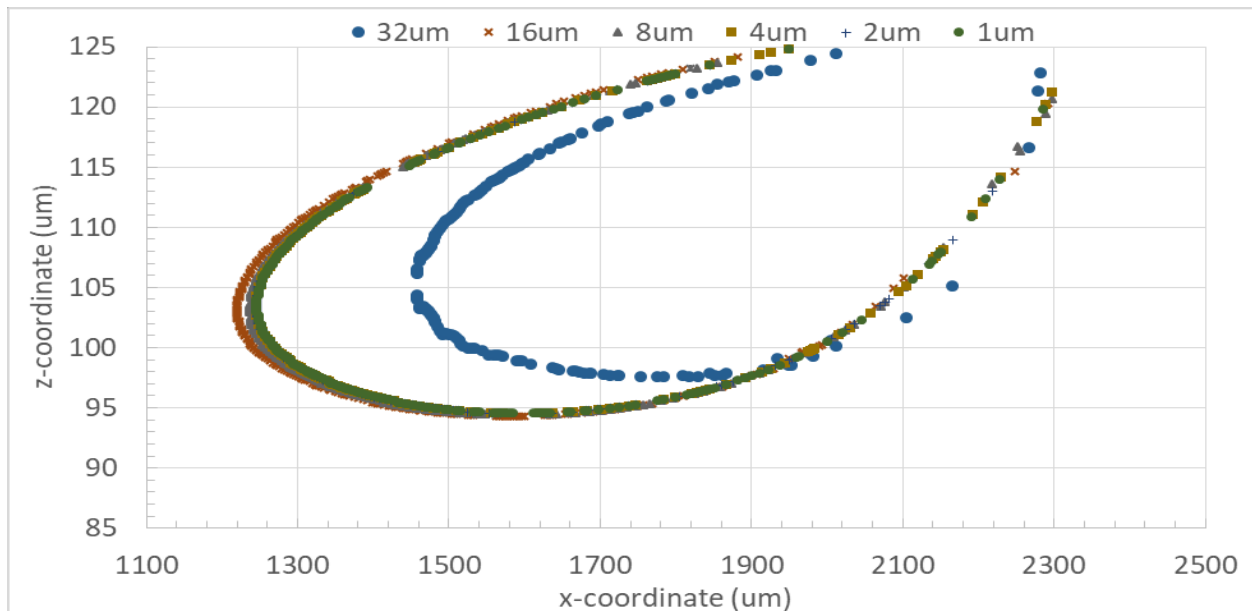
Figure 3.5: T=700K Isotherm during mesh convergence analysis. Taken at t=0.0052, using constant material properties for PMMA as described previously

interpolated within COMSOL. The isotherm appears to converge quickly after 32 um, with virtually no distinguishable difference at 4um and smaller. A similar result is found in figure 3.6, where the temperature is very consistent after 32um.

3.5.2. Channel Depth Convergence
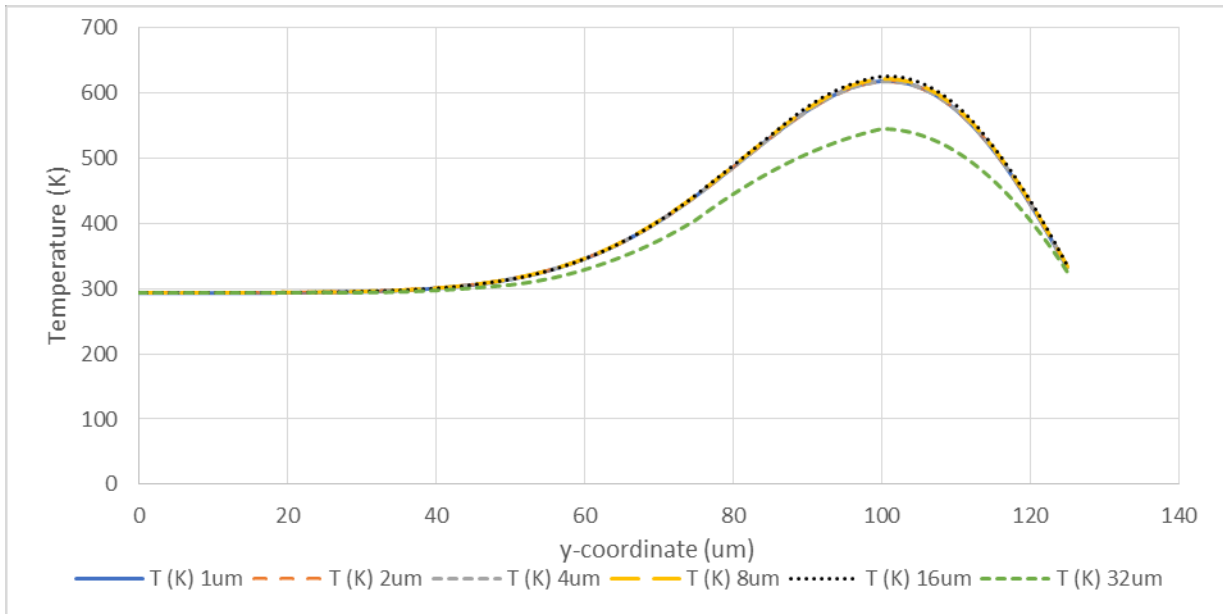
Figure 3.6: Temperature as a function of depth in the material at a given cross-section. Taken at x=1000um, t=0.0052s. Material properties for PMMA are used for all cases considered for comparison.

The second parameter considered for convergence is the depth of cut itself, by taking the maximum depth at which the temperature reaches 700 K and recording it. The results of this, shown in figure 3.7, indicate that the depth does not change after size 4 um. According to all convergence criteria presented, the results converge to the same value starting at 4 um or smaller. By looking at all of these results, it is clear that the 4 um mesh size is the best option and is used in all 2D simulations presented.
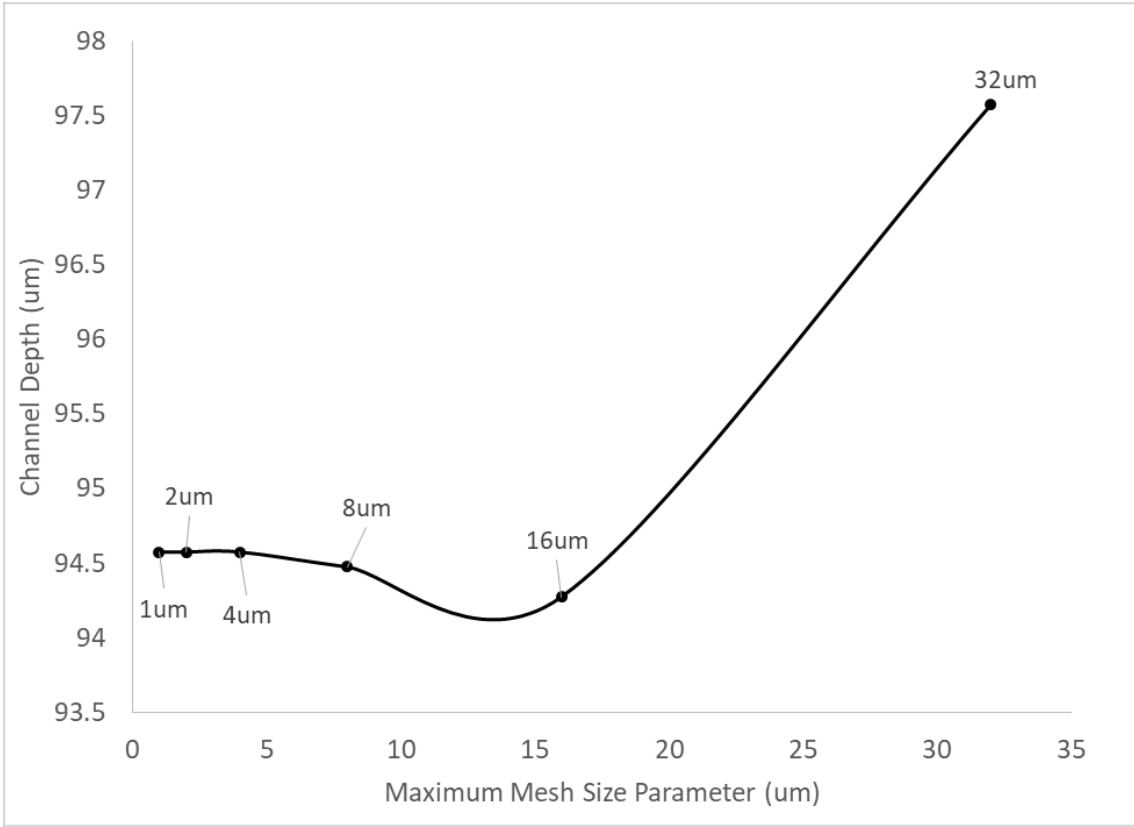
Figure 3.7: Channel depth determined from each mesh.

Chapter 4: Results and Discussion

The results are split into two main categories, the laser system parameters and the thermal parameters. First, the three dimensional model is used to investigate the effect of laser spot size on the depth and shape of the fabricated channel. The 3D model was then used to investigate the effect of the laser scanning speed on the channel shape. The effect on channel depth was also investigated, using the two dimensional model. This allowed for a parametric investigation of depth with respect to both laser speed and power. Second, a parametric study on thermal properties of the system was conducted using the 2D model. The convection coefficient of the ablation process, as well as the heat capacity and thermal conductivity of the substrate, are all considered. For each parameter, several values are considered for a range of laser power settings. In all of these cases, the effect of depth is investigated.

4.1. Material Properties and System Parameters

To establish consistency between all the results, the material properties of PMMA were used in all cases unless otherwise specified. This was done because PMMA has received the most attention in literature on the use of CO_2 lasers for fabrication in microfluidics. The values used are found in table 4.1 below. In addition to the material properties, the laser and other system parameters must also be specified. These values are given in table 4.2. The cut length parameter specified determines the length of the channel being modeled. The size of the model is defined accordingly.

Table 4.1: Material Properties used within the heat transfer model. The constant values given are for PMMA [43].

Property	Units	Constant Value	Parametric Range
Thermal Conductivity, k	$Wm^{-1}K^{-1}$	0.19	0.019 - 3.8
Specific Heat, C_P	$Jkg^{-1}K^{-1}$	1477	500 - 3000
Density, ρ	kg/m^3	1180	-
Emissivity, ε	1	0.91	-
Absorption Coefficient (at 10.6um),α	m^{-1}	1×10^6	-

Table 4.2: System parameters used within the model

Property	Units	Constant Value	Parametric Range
Laser Power Output, I_0	W	65	-
Beam Radius, w_0	um	92.5	92.5 - 500
Laser Velocity, V_L	mm/s	381	50 - 500
Cut Length	mm	2	-
Convection Coefficient, h	$Wm^{-2}K^{-1}$	1×10^5	$2.5 - 5 \times 10^5$

4.2. Effect of Laser System Parameters on Resulting Channel

4.2.1. Laser Parameter: Spot Size

The first laser system parameter considered is the size of the laser beam, described by the spot size. For the purposes of modelling, it is assumed that the substrate is located at a distance away from the focal point of the laser light such that distance d as shown in figure 4.1 is equal to zero. This means that the laser beam is focused on the surface of the substrate, at a distance equal to the focal length f of the focusing lens where the
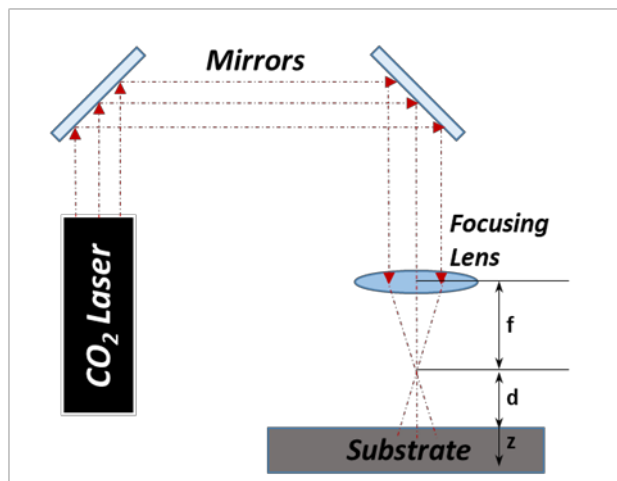

Figure 4.1: Schematic of laser set up. Where f is the focal length of the focusing lens, and d is the distance between the substrate and the focusing length.

beam converges to a minimum radius value. Thus, the radius specified within the model is equal to the waist radius, the minimum radius of the beam. Here, waist radius values between 50-500μm are considered. For these waist radii, it can easily be verified that the calculated radius value at distances up to 100um away from the substrates varies by at most 2%, as shown in figure 4.2b. This shows that the radius value can reasonably be taken as a constant.

Until now, the only case considered has been where the substrate is located exactly at the focal length f, where d=0 referring to figure 4.1 above. However, if the substrate is not exactly at this focal distance, the beam will effectively have a larger radius. The corresponding radius, w can be found from:

$$d = \frac{\pi w_0^2}{\lambda} \sqrt{\left(\frac{w}{w_0}\right)^2 - 1} \tag{4.1}$$

Here, the value of d corresponding to a given beam radius w can be found, as shown in figure 4.2a and λ is the wavelength of the laser. This corresponds to placing the substrate at a distance f+d away from the focusing lens, with a beam of effective radius w irradiating it. This means that
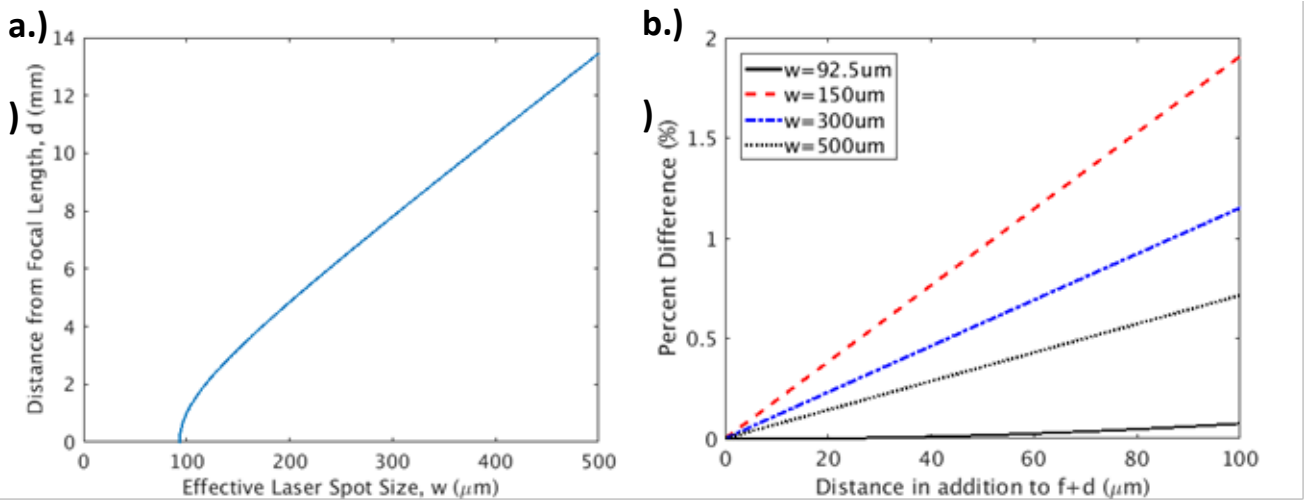

Figure 4.2: Calculation of effective radius, w for use within model. a) Effective distance away from focal length for a given desired laser spot size. The min b) Variation of spot size along the depth of the channel

28

even without adjusting the lens, the radius of the beam can be effectively set by changing the

distance between the lens and the substrate according to figure 4.2a. Here, the minimum spot

size is the waist radius, where w=92.5um is shown. This gives two possible methods for

controlling the spot size in application, one by changing the optical set up such that the beam is

more tightly or loosely focused, or two by varying the distance of the substrate to the piece.

To investigate the effect of spot size on the resulting channel, several spot size values are

considered. All system parameters, other than beam radius, are set to the values found in tables

4.1 and 4.2. The laser power is set to a fraction of the total power of the laser. In these cases,

40% of the total power (26W) is used. The results of varying the radius and laser power on depth

are shown in figure 4.3. The depth is determined from the temperature profile. The maximum

depth at which the material reaches a temperature of 700 K is used. The results show that when

the beam radius is increased, the depth is decreased. This is due to the energy of the laser beam
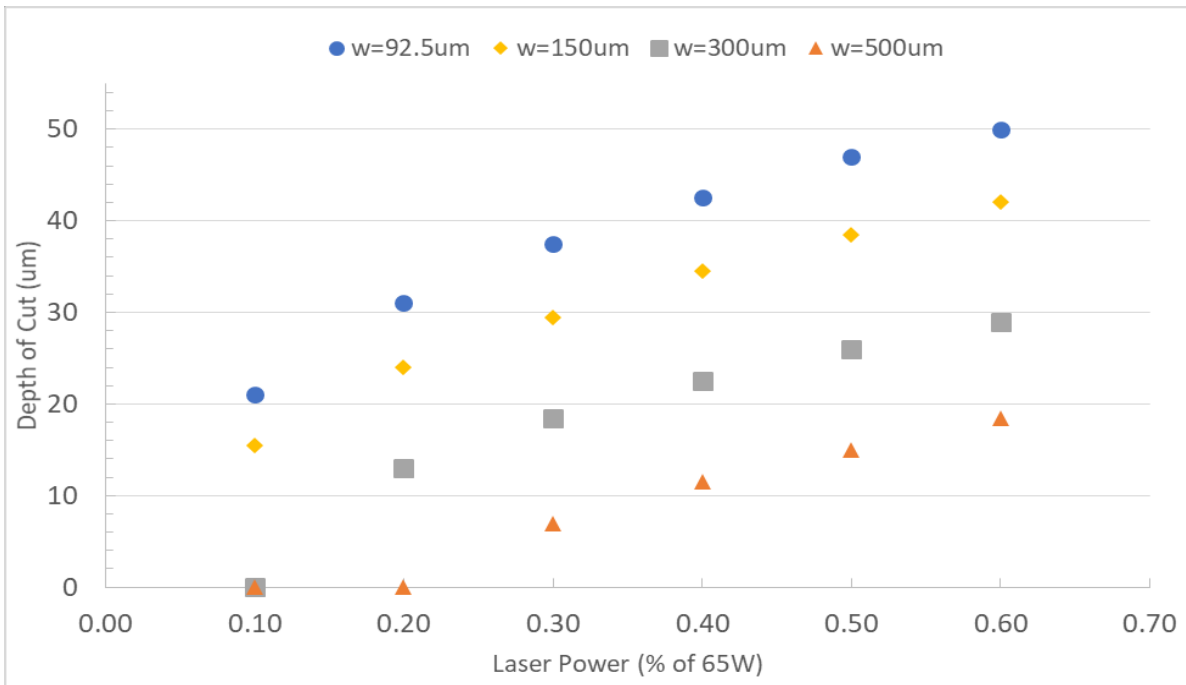

Figure 4.3: Channel depth as a function of laser power for various laser beam radii

being distributed throughout a larger area, decreasing the intensity of the heat added. This decreased intensity prevents the heat from penetrating further into the material. The effect of varying the laser power is also shown in figure 4.3. For the range of values given, the effect of laser on depth is mostly linear. This holds true for all radius values considered. For lower power and larger radius, some values do not show any material removal. This is indicated by a depth of cut of 0. Therefore there is a minimum power needed for creating a channel on the PMMA substrate.

Figure 4.4 shows the cross-sectional profiles of the channels cut by the laser. These profiles are generated by taking a cross-section normal to the axis of the laser's path. The temperature data is evaluated on this cross-section as a rectangular grid, and the minimum and maximum x-coordinate that reaches a temperature of 700K for each y-coordinate is recorded. These points indicate the outer edges of the removed material, giving the shape of the channel cut out of the material. For each radius, these are plotted and compared to a gaussian curve fit, generated using the Curve Fitting Toolbox in MATLAB R2016A. More details of the curve fitting can be found in appendix A.

From these results, it is shown that the channel cut by the laser is very closely approximated by a gaussian function for smaller radius values (92.5 and 150um). For smaller radii, the laser light is more focused, resulting in less loss of power concentrated on the surface. However, as the radius increases to 300um, and especially 500um, this fitting begins to lose its accuracy. At higher radii, the laser is less focused and scattered. One thing to note is that on all 4 radii, the width is shown to decrease near the top of the channel. This is likely due to the mesh not being fine

enough in the 3D model, as well as the time stepping. This issue is resolved later using the 2D model, as explained in the mesh convergence analysis in the previous section.

When plotted together, effect of decreased depth with increased radius is very clear. The heat is spread out in a much larger area, creating an increasingly shallow and wide channel. By varying the beam radius, either by changing the vertical distance between the laser and the material or by varying the optical set up, the depth and width of a channel can be set.

4.2.2. Laser Parameter: Scanning Speed

The second laser parameter considered is the laser scanning velocity during the ablation process. Understanding this effect, along with the effect of laser power, is important for understanding the extent of flexibility a CO_2 laser system offers for fabrication. During laser cutting, the speed of the laser is generally held fixed for consistent results. For the same material and power, adjusting the scan speed can also affect the resulting channel, since it will alter the exposure time to the laser at all points affected by the laser. Though it is not presently modelled here, it has been reported in literature that the laser scanning speed influences the roughness of the fabricated channel, with increased roughness for decreased speeds [13, 38, 39].

First, the effect of laser speed on depth of the channel is investigated. This is done using a 2D model so that this effect can be considered for a range of power settings. The results of varying the laser scan speed and power the depth is presented in figure 4.5. When the velocity is increased, the channel depth decreases. When the laser passes over an area faster, the total amount of energy imparted on the material in a given area is reduced, resulting in lower cut depths. It is important to note that, for a wide range of depths, various power and speed

31

A.) 92.5µm

B.) 150µm

C.) 300µm
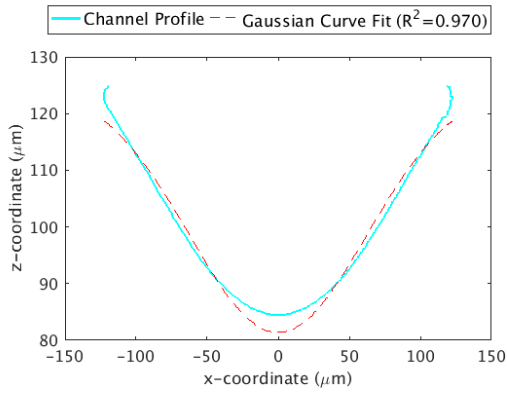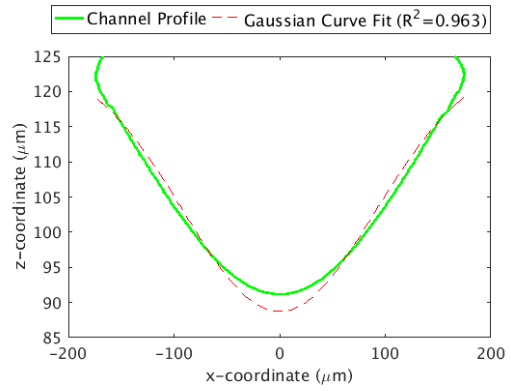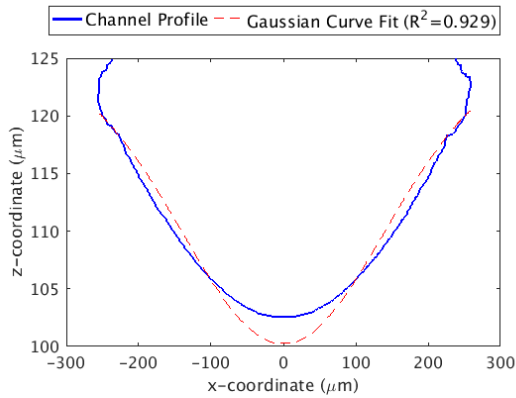
D.) 500µm
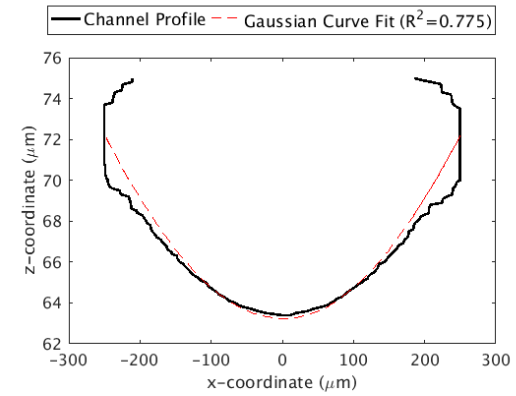
E.) All profiles together
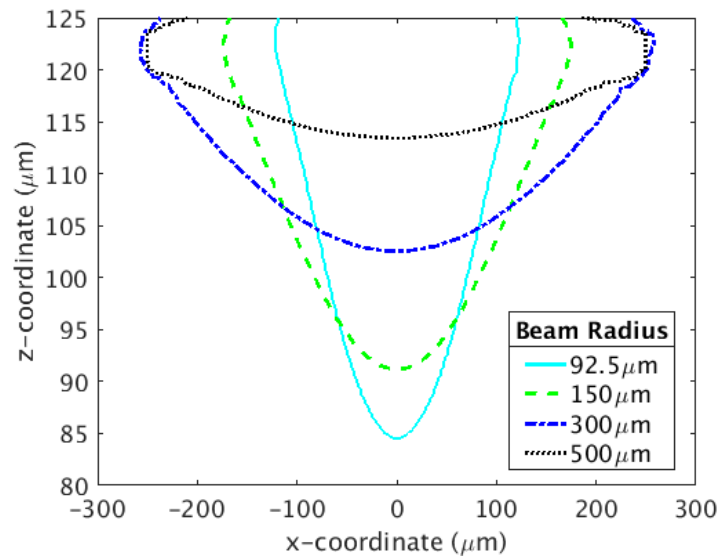
Figure 4.4: Depth of the channel cut out by the laser for various laser beam radii. Parts A-D contain the channel profile for the labeled beam radii, 92.5, 150, 300, and 500µm respectively. A gaussian curve fit is plotted along with each one. Part E contains all four profiles plotted against each other.
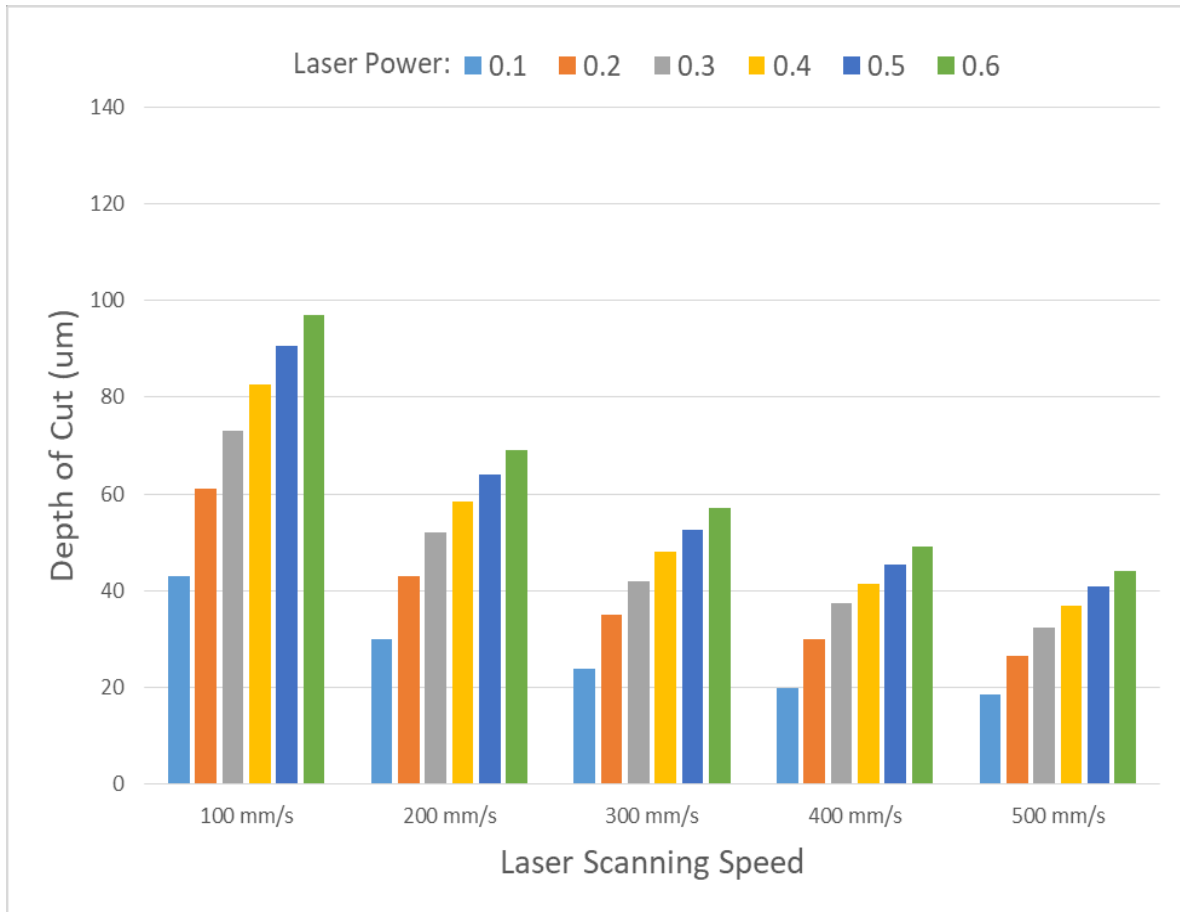
Figure 4.5: Depth vs power for laser scan velocity between 50-500 mm/s. For each laser scan velocity, the depth is presented in order of increasing laser power.

combinations can result in the same depth. For example, a power setting of 10% with a laser

speed of 100mm/s gives the same depth as setting the power to 20% with a speed of 200mm/s

However, it is important to note that other experimental research on laser fabrication has found

that when the scan speed is too low, the roughness of the channels can be significant. In these

cases, the researchers recommend minimum scan speeds in order to avoid these concerns.

According to Klank et al. [38], the excess roughness is a result of large amounts of re-solidified

material in the channels. They recommend that for a power setting of 52 W (80%), the speed

should be at least 300 mm/s, and for a power setting of 6.5 W (10%) the speed should be at least

80 mm/s.

In addition to the concern of roughness, the overall cross-sectional profile of the channel can also change. For two different speed and power combinations resulting in the same measured depth, the channel profile can be narrower or wider depending on the scan speed as well. To investigate this effect, the 3D model is used to find the channel cross-section, similarly to what was done for the spot size investigation. Using this, the effect that varying the scanning velocity has on the profile is determined, by comparing several different scan speeds while maintaining the same laser power. The results of this are shown in figure 4.6.

Figure 4.6: Depth of the channel for laser scan velocity between 100-500 mm/s. The resulting channel from several laser scan speeds are compared on the same plot. In all cases shown here, the power is set to 40%

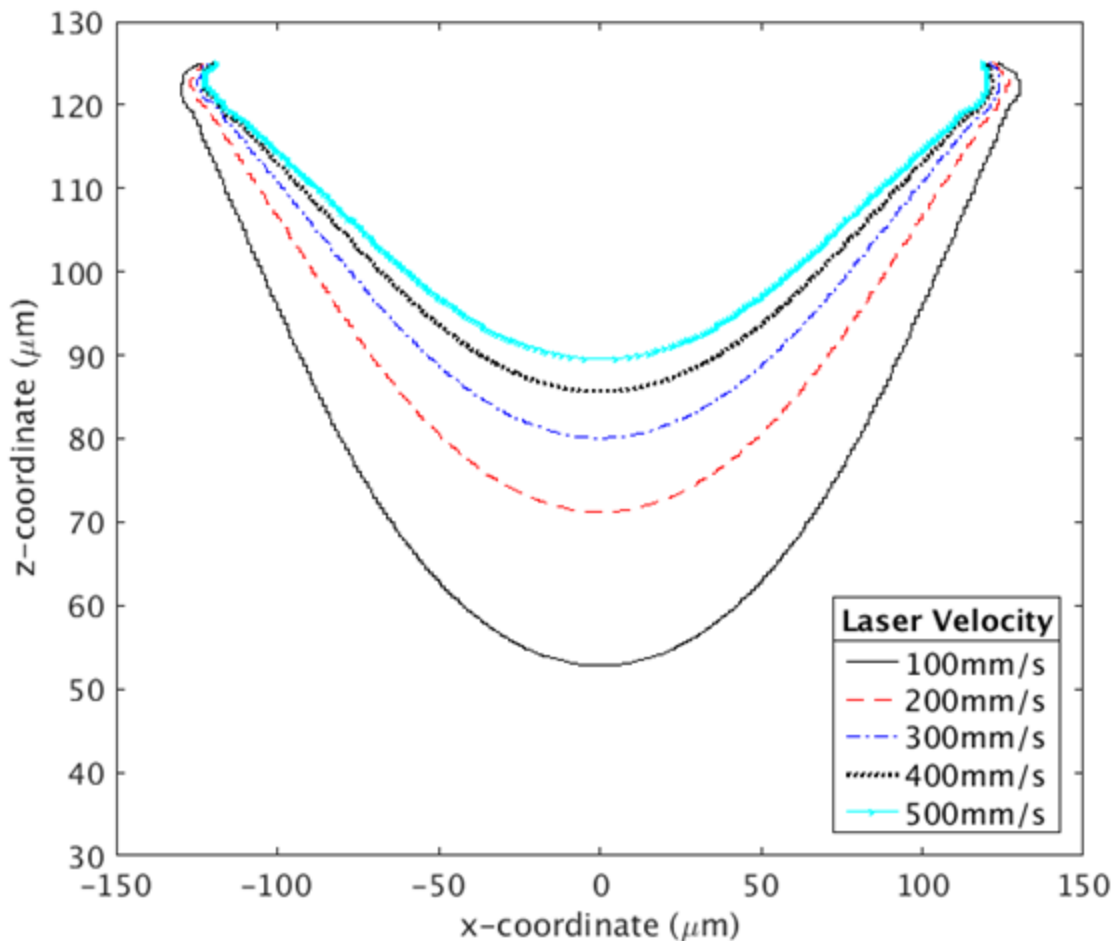From the figure, it is clear that when the laser scan speed is changed, the width of the channel remains approximately the same. However, as the scan speed increases, the depth of the channel does change, as described previously. The individual profiles along with Gaussian curve fittings, similar to those shown for the spot size in figure 4.4, can be found in the appendix B. Since the depth change while maintaining the same width, various aspect ratios can be obtained for the channel simply by varying the laser speed.

4.3. Parametric Study of the Effects of Thermal Properties on Channel Depth

4.3.1. Parametric Investigation of the Convection Coefficient

4.3.1a. Validation of simplification to 2D model

The results of the parametric investigation of the convection coefficient are found using both 3D and 2D models for several cases considered. This is done to validate the use of a 2D model used in considering the laser velocity in the previous section, as well as for the remainder of the parametric study. A range of values for the convection coefficient are considered, between $10,000 - 500,000$ $Wm^{-2}K^{-1}$. As described in the chapter on theory and modeling, the convection coefficient values are taken to be on the same order of magnitude as pool boiling heat transfer coefficients [46, 48]. This choice is made due to the phase change that is also occurring in the case considered here. For each of these values, the laser power is allowed to varying between 10% and 60% of the maximum power output of the laser. The predicted channel depth is used to compare and validate these results. The results of this comparison are presented in table 4.3.

Table 4.3: Error between the 3D and 2D models for the reported channel depths. All parameters, other than the convection coefficient, are set to the values specified in tables 4.1 and 4.2 in both models

P_0 (% of total laser power)	h=10000 (Wm^{-2}K^{-1})	h=50000 (Wm^{-2}K^{-1})	h=100000 (Wm^{-2}K^{-1})	h=250000 (Wm^{-2}K^{-1})	h=500000 (Wm^{-2}K^{-1})	Average error
0.10	2.70%	0.97%	0.00%	0.00%	0.00%	0.73%
0.20	2.08%	1.41%	0.83%	0.00%	0.00%	0.86%
0.40	2.22%	3.23%	2.44%	-	-	2.63%
0.60	0.81%	2.33%	2.04%	1.18%	-	1.59%

The actual values for the depth found using the 3D model can be found in Appendix C, while the values for the 2D model are reported later in this section. The error found in all the cases considered is well within reason, being less than 4%. Additionally, it should be noted that the results of the 3D model presented in figure 4.4 found in the preceding section indicate that the channel profile is symmetric about the centerline of the channel. This implies that there is no heat flux in the normal direction of the 2D plane considered, so that all of the heat flux in the 2D model is confined within the plane.

The main concern of these investigations is to effectively model the laser cutting process, to find reasonable and effective approximations of the resulting channels in various materials. The main weakness of the 2D model is that it cannot predict the profile of the channel cut. As seen in the previous 3D model however, it has already been established that the laser power and beam radius effect the geometric size of the channel, while maintaining an overall gaussian shape. It is reasonable to expect that the channel profile will remain gaussian, since this is directly connected to the gaussian nature of the laser heat source being applied. As a result, looking at the channel depths indicated by the 2D model, along with the established gaussian nature of the channel,

provides valuable insight without requiring a computationally expensive, fully 3D parametric study.

4.3.1b. Parametric Investigation of Convection Coefficient

The full results of the 2D parametric study are shown in figure 4.7. Values for a wider range of convection coefficients between 250 and 5×10^5 $Wm^{-2}K^{-1}$ are used, with power settings between 10% and 60%. A value of 250 $Wm^{-2}K^{-1}$ is used to compare to the significantly higher values also considered. This value is found as the upper bound estimate on the convection coefficient found using established convection coefficient correlations, reported by Tresansky et al. [43] in the development of their model.
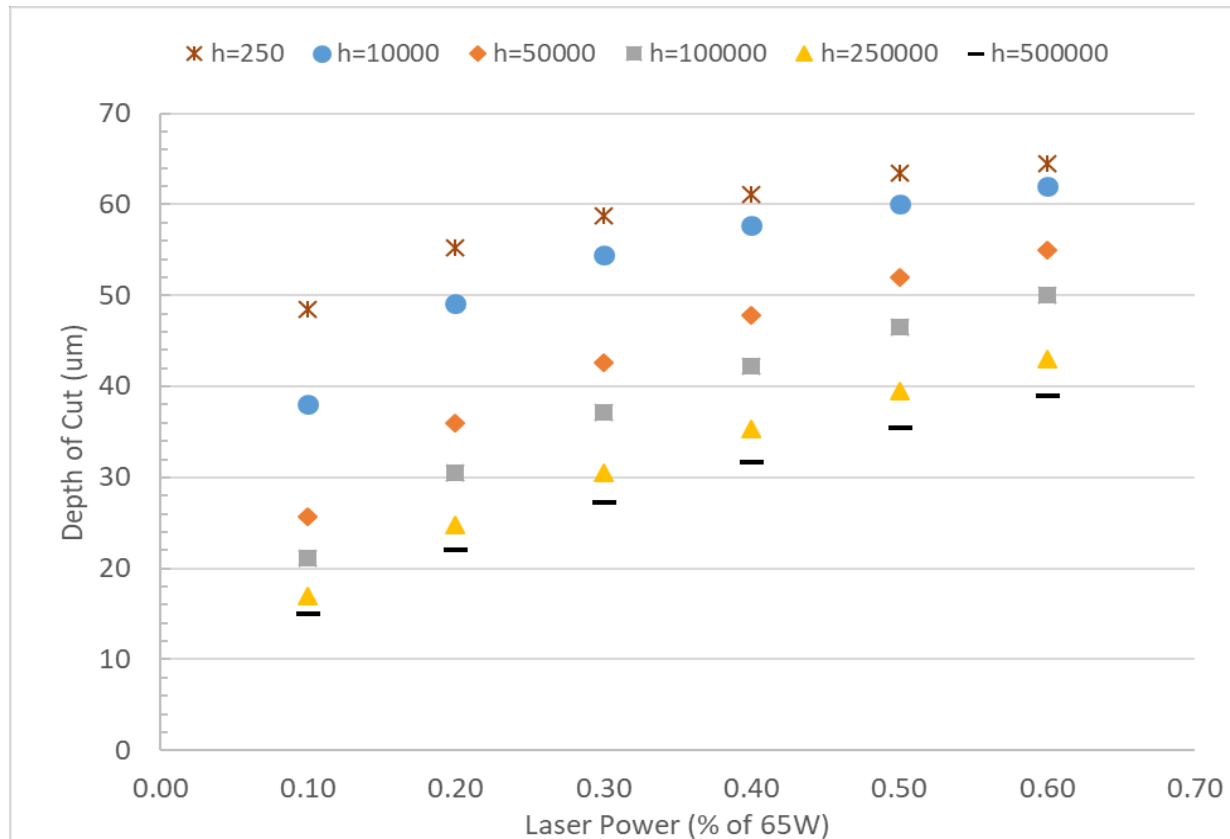

Figure 4.7: Depth vs laser power for various convection coefficients. All material and system properties, other than convection coefficient, are set to the values found in Tables 4.1 and 4.2

The use of 250 Wm^{-2}K^{-1} in this model is clearly inadequate at accounting for the temperature within the material. Using this value, very little variation in depth with power is found. However, it is clear that from the existing experimental literature that the power has a significant influence on depth [13, 38, 39] In general for lower convection coefficient values, the depth does not vary much with increased laser power, while for larger coefficients, the laser power has a more pronounced effect. Overall though, increases in convection coefficient has the effect of decreasing the depth indicated by the model. The effect of the convection coefficient is to model the amount of heat removed not only by direct natural convection at the surface, but to also approximate the effect of additional heat escaping the bulk material. This heat escapes when melting and vaporization of the material occurs, and much of the vaporized material produced escapes the modelled area. Without a way to account for this loss, the total amount of heat within the model would be vastly overestimated. The use of convection coefficient to account for this is far more computationally efficient, compared to more direct ways of accounting for phase change. It is important to note that currently, more information is necessary to determine a convection coefficient that corresponds to this case. What this does show however, is that higher values of convection coefficient, could very likely be used in future models.

4.3.2. Parametric Investigation of Specific Heat

4.3.2a. Constant Specific Heat

The specific heat of a material has a significant impact on how a material responds to laser cutting. In order to accurately predict whether laser fabrication will be appropriate to use on a material, the effect of specific heat on the resulting channel needs to be understood. Here, a

range of constant specific heat values are considered between 500-3000 Jkg^{-1}K^{-1} at various laser powers. The resulting channel depths are shown in figure 4.8.

The results show that for lower specific heat values, the depth is much more sensitive to the effect of laser power. Also, the effect of specific heat is more pronounced at higher laser powers. It can be noted that even when the specific heat is higher, the same depths can be achieved simply by using higher power setting on the laser. This means that the same channels should be achievable with different materials simply by adjusting the power to account for this.
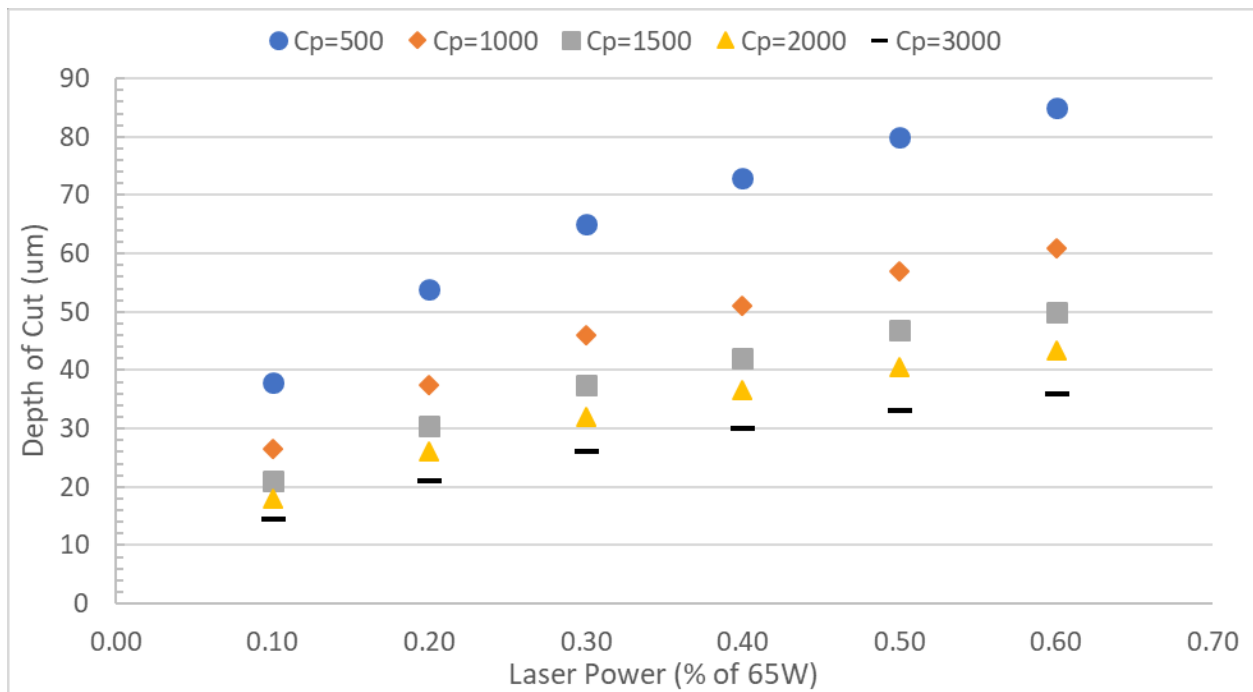
Figure 4.8: Depth vs laser power for various constant specific heat values. All material and system properties, other than specific heat, are set to the values found in Tables 4.1 and 4.2

4.3.2b. Temperature Considerations for Specific Heat

Although a constant specific heat was used in this model, it should be noted that the effective specific heat varies considerably during a phase change. A portion of the absorbed laser heat will go into the phase changes, from solid to liquid and liquid to gas. This heat is referred to as latent

heat, and the amount lost to this can be significant. For a more thorough investigation, the implementation of phase change is also considered here.

The phase change is implemented as a temperature dependent specific heat. Within COMSOL, smoothed step functions are used to implement the change in values at the point at which phase change occurs. Smoothed step functions are used due to issues with evaluation in COMSOL while using discontinuous functions. The latent heat is also distributed over a range of temperatures as well, ending around the point at which the phase change is known to occur. The value for the latent heat, as well as the temperature range used in implementation were found in literature [43].

$$C_p = C_{p,solid} \left(1 - H(T)\right) + \Delta h_{Latent} \, D(T) + C_{p,vapor} \, H(t) \qquad (4.2)$$

Where H(T) is the smoothed Heaviside function centered at the vaporization temperature, and D(T) is a function used to distribute the latent heat of phase change across the phase change interval. The depth of cut resulting from this consideration are shown in table 4.4. The cut depth for the constant solid specific heat is also shown in the table. If the specific heat value used in the model is taken to be constant, the solid value would be the most reasonable choice. However, as shown in the table, the case that considers temperature dependence shows to be on average 10% different. This difference is far too significant to be ignored, meaning that for a computational model such as this one, it is clear that the temperature dependence of specific heat must be accounted for.

Table 4.4: Depth of Cut for temperature dependent specific heat

	0.1	0.2	0.3	0.4	0.5	0.6
$C_p(T)$	19	28	34	38	42	45
$C_{p, solid}$	21.0	30.5	37.5	42.0	47.0	50.0
% Difference	10.00%	8.55%	9.79%	10.00%	11.24%	10.53%

4.3.3.   Parametric Investigation of Thermal Conductivity

The thermal conductivity is a measure of how well heat can move through material. In the case

of laser heating, the heat is localized to a very small region of intense heat. This is made possible

by a low conductivity, so that the heat is not able to spread far from the initially irradiated region.

Since the thermal conductivity is related to how well heat spreads throughout a material, it

should have an impact on the resulting channel depth. To better understand and predict the

resulting channel on different materials, the effect of thermal conductivity needs to be

understood. Here, a wide range of thermal conductivity values are considered across several

orders of magnitude, between 0.025 and 5 $Wm^{-1}K^{-1}$.

From figure 4.9 it is clear that higher the conductivity is, the deeper the channel that is cut. This

is because higher thermal conductivity corresponds with an easier spreading out of heat,

meaning that heat can reach further and further down before it is ultimately removed into the

air by convection. Figure 4.9 contains the lower range values of thermal conductivity that are

considered in this study, up to 0.3 $Wm^{-1}K^{-1}$. The results for the higher range of values can be

found in Appendix D. In the case of polymers, the range of values contained here are the most

reasonable values for polymers commonly considered for microfluidics. The thermal conductivity

of polymers for the most part fall in the range of 0.1-0.3 Wm $^{-1}$K^{-1} [49]. PMMA for example, has

a value of 0.19 Wm^{-1}K^{-1}, as reported in previous chapters. Values outside this range, both lower

and higher, are considered still for completeness. Although most materials will fit in the smaller

range, it is still important to understand how the limiting cases of application work. Again, this

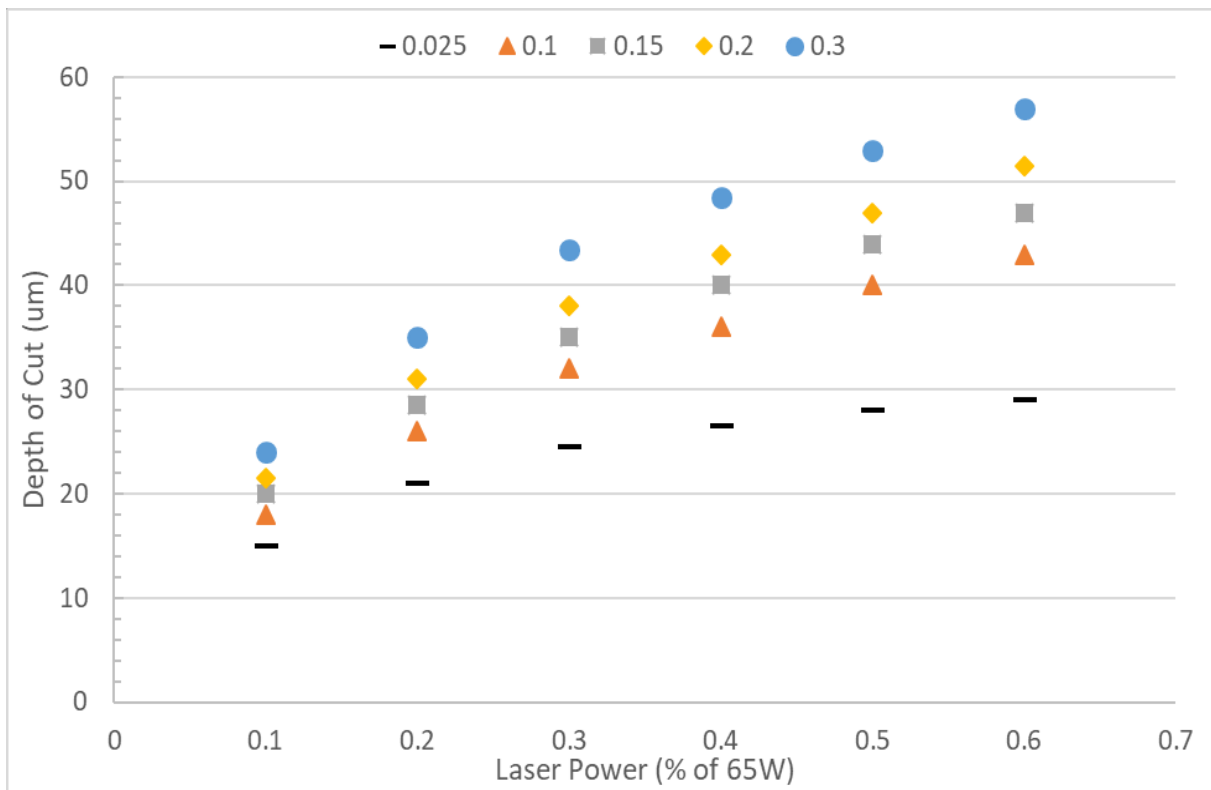information can be found in appendix D.

Figure 4.9: Depth vs laser power for various thermal conductivity values. All material and system properties, other than thermal conductivity, are set to the values found in Tables 4.1 and 4.2. The results are split into two graphs, a) Lower values, and b) Higher values.

Chapter 5: Conclusions and Future Work

5.1.   Conclusions

The purpose of this thesis was to more thoroughly investigate CO_2 laser fabrication in microfluidics. This was accomplished through numerically modelling the process, to determine the effect of individual parameters on the resulting fabricated channel. The effect of three main laser system parameters were considered, the laser spot size, the laser scanning speed, and the laser power. Additionally, three thermal properties were considered: the convection coefficient, the specific heat of the substrate material, and the thermal conductivity of the substrate material.

It was found that the laser system parameters can be used to control and eventually fine-tune the fabrication process for both channel width and height. The first parameter considered was the laser spot size. It was shown that this value can be effectively controlled in two ways by the user: by varying the optics of the focusing lens, or by varying the position of the laser cutting stage. The spot size affects both the width and height of the channel, with smaller spot size being associated with narrower, deeper channels, and larger spot sizes with shallower, wider channels. The laser scanning speed has very little effect on the width of the channel, while having a much more significant effect on the depth. Lower scanning speeds are associated with a deeper channel, while higher scan speeds result in shallower channel. The depth decreases non-linearly with increasing laser scan speed. A similar trend is seen with laser power, where the depth increases non-linearly with increasing power. By considering the effects of all three parameters together, it would be possible to a channel with a desired width and depth by adjusting the laser

spot size, speed, and power accordingly. In addition, several thermal properties were investigated. A summary of all the findings are presented below:

- Laser System Parameters:

    a) The laser spot size affects both the depth and width of the channel. Larger laser spot size creates wider and shallower channels.

    b) The laser scanning speed mainly affects the depth, while having little to no impact on the width of the channel. If the laser scanning speed is higher, the depth of cut is decreased.

    c) The laser power strongly affects the depth of the channel. Laser power and depth of channel has linear relation

- Thermal Parameters:

    a) Very high convection coefficients more accurately describe the system.

    b) Constant effective specific heat values are not sufficient for the mathematical modelling. A temperature dependent expression of specific heat is more appropriate.

    c) Higher specific heat materials reduce the cut depth, while higher thermally conductive materials increase the cut depth

Most existing literature at this point as focused on the use of CO_2 laser fabrication on PMMA, though a few other polymers have begun to be considered and still more have still yet to be tested. By considering different possible material property values, it is possible to predict how channels will turn out in many of these other materials. By adjusting the laser system parameters, the same desired channel with matching dimensions can be cut into different materials.

5.2. Future Work

Much work is still needs to be done to fully model the laser fabrication process. The work presented here describes the general trends and results of various system parameters and material properties.

One weakness of the model is that it does not predict the roughness of the channel. A more comprehensive model including the full effects of phase change, and the interaction between the multiple phases that exist during the process would be necessary to do so. This would be extremely computationally intensive and likely not worth investigating currently. Such a model would be incredibly useful however. Another option is an extension of previous experimental studies on roughness to include other potential material is recommended. Once materials are found to either work or not work based on roughness, the model can then be applied.

Summary of recommended future work:

1. Develop mathematical modeling to incorporate measurement of roughness or prediction of roughness value and its correlation with process parameters.
2. Develop mathematical modeling that can incorporate phase change transition and predict curing time of laser ablation

References

[1]   G. Whitesides, "The origins and the future of microfluidics," *Nature,* vol. 442, no. 27, pp. 368-373, 2006.

[2]   G. Whitesides and A. Stroock, "Flexible Methods for Microfluidics," *Physics Today,* vol. 54, no. 6, pp. 42-48, 2001.

[3]   G. Lee, S. Chen, G. R. Huang and W. Sung, "Microfabricated plastic chips by hot embossing methods and their applications for DNA separation and detection," *Sensors and Actuators B: Chemical,* vol. 75, no. 1, pp. 142-148, 2001.

[4]   U. Attia, S. Marson and J. Alcock, "Micro-Injection Moulding of Polymer Microfluidic Devices," *Microfluidics and Nanofluidics,* vol. 7, no. 1, 2009.

[5]   R. Thanu, "Design, analysis and fabrication of hot embossing microfabrication system," University of Texas at Arlington, 2003.

[6]   T. Kim, K. Campbell, A. Groisman, D. Kleinfeld and Schaffer, "Femtosecond laser-drilled capillary integrated into a microfluidic device," *Applied Physics Letters,* vol. 86, no. 20, p. 201106, 2005.

[7]   D. Wolfe, J. Ashcom, J. Hwang, C. Schaffer, E. Mazur and G. Whitesides, "Customization of Poly(dimethylsiloxane) Stamps by Micromachining Using a Femtosecond-Pulsed Laser," *Advanced Materials,* vol. 15, no. 1, pp. 62-65, 2003.

[8] G. M. Whitesides, "The origins and the future of microfluidics," *Nature,* vol. 442, no. 27, pp. 368-373, 2006.

[9] N. Gottschlich, S. Jacobson, C. Culbertson and M. Ramsey, "Two-Dimensional Electrochromatography/Capillary Electrophoresis on a Microchip," *Analytical Chemistry,* vol. 73, no. 11, pp. 2669-2674, 2001.

[10] R. Su, J. Lin, F. Qu, Z. Chen, Y. Gao and M. Yamada, "Capillary electrophoresis microchip coupled with on-line chemiluminescence detection," *Analytica Chemica Acta,* vol. 508, no. 1, pp. 11-15, 2004.

[11] J. Mellors, V. Gorbounov, R. Ramsey and J. Ramsey, "Fully Integrated Glass Microfluidic Device for Performing High-Efficiency Capillary Electrophoresis and Electrospray Ionization Mass Spectrometry," *Analytical Chemistry,* vol. 80, pp. 6881-6887, 2008.

[12] M. Yu, Q. Wang, J. Patterson and A. Woolley, "Multilayer Polymer Microchip Capillary Array Electrophoresis Devices with Integrated On-Chip Labeling for High-Throughput Protein Analysis," *Analyical Chemistry,* vol. 83, no. 9, pp. 3541-3547, 20011.

[13] T. Hong, W. Ju, M. Wu, C. Tai, C. Tsai and L. Fu, "Rapid prototyping of PMMA microfluidic chips utilizing a CO2 laser," *Microfluidics and nanofluidics,* vol. 9, no. 6, pp. 1125-1133, 2010.

[14] D. Schrum, C. Culbertson, S. Jacobson and J. Ramsey, "Microchip Flow Cytometry Using Electrokinetic Focusing," *Analytical Chemistry,* vol. 71, no. 19, pp. 4173-4177, 1999.

[15] Y. Liu, C. Rauch, R. Stevens, R. Lenigk, J. Yang, D. Rhine and P. Grodzinski, "DNA amplification and hybridization assays in integrated plastic monolithic devices," *Analytical Chemistry,* vol. 74, no. 13, pp. 3063-3070, 2002.

[16] L. Kricka and P. Wilding, "Microchip PCR," *Analytical & Bioanalytical Chemistry,* vol. 377, no. 5, pp. 820-825, 2003.

[17] W. Gan, Y. Gu, J. H. Han, C. Li, J. Sun and P. Liu, "Chitosan-Modified Filter Paper for Nucleic Acid Extraction and "in Situ PCR" on a Thermoplastic Microchip," *Analytical Chemistry,* vol. 89, no. 6, pp. 3568-3575, 2017.

[18] M. Chun and I. Lee, "Rigorous estimation of effective protein charge from experimental electrophoretic mobilities for proteomics analysis using microchip electrophoresis," *Colloids and Surfaces A: Physicochemical and Engineering Aspects,* vol. 318, no. 1-3, pp. 191-198, 2008.

[19] J. Liu, T. Pan, A. Woolley and M. L. Lee, "Surface-Modified Poly(methyl methacrylate) Capillary Electrophoresis Microchips for Protein and Peptide Analysis," *Analytical Chemistry,* vol. 76, no. 23, pp. 6948-6955, 2004.

[20] C. Chung, T. Shih, C. Chang, C. Lai and B. H. Wu, "Design and experiments of a short-mixing-length baffled microreactor and its application to microfluidic synthesis of nanoparticles," *Chemical Engineering Journal,* vol. 168, no. 2, pp. 790-798, 2011.

[21] C. Lin, C. Tsai and L. Fu, "A rapid three-dimensional vortex micromixer utilizing self-rotation effects under low Reynolds number conditions," *Journal of Micromechanics and Microengineering,* vol. 15, pp. 935-943, 2005.

[22] A. Hatch, D. Pesko and S. Murthy, "Tag-Free Microfluidic Separation of Cells against Multiple Markers," *Analytical Chemistry,* vol. 84, no. 10, pp. 4618-4621, 2012.

[23] S. Patel, D. Showers, P. Vedantam, T. Tzeng, S. Qian and X. Xuan, "Microfluidic separation of live and dead yeast cells using reservoir-based dielectrophoresis," *Biomicrofluidics,* vol. 6, no. 3, p. 034102, 2012.

[24] S. Kim, F. Wang, M. Burns and K. Kurabayashi, "Temperature-Programmed Natural Convection for Micromixing and Biochemical Reaction in a Single Microfluidic Chamber," *Analytical Chemistry,* vol. 81, no. 11, pp. 4510-4516, 2009.

[25] E. Sackmann, A. Fulton and D. Beebe, "The present and future role of microfluidics in biomedical research," *Nature,* vol. 507, no. 7491, p. 181189, 2014.

[26] J. C. McDonald, C. Duffy, J. R. Anderson, D. Chiu, H. Wu, O. A. Schueller and G. Whitesides, "Fabrication of microfluidic systems in poly(dimethylsiloxane)," *Electrophoresis,* vol. 21, pp. 27-40, 2000.

[27] R. Mukhopadhyay, "When PDMS isn't the best," *Analytical Chemistry,* vol. 79, pp. 3248-3253, 2007.

[28] E. Berthier, J. Warrick, H. Yu and D. J. Beebe, "Managing evaporation for more robust microscale assays Part 1. Volume loss in high throughput assays," *Lab on a Chip,* vol. 8, no. 6, pp. 852-859, 2008.

[29] D. Eddington, J. Puccinelli and D. Beebe, "Thermal aging and reduced hydrophobic recovery of polydimethylsiloxane," *Sensors and Actuators B,* vol. 114, pp. 170-172, 2006.

[30] J. Lee and C. G. Park, "Solvent Compatibility of Poly(dimethylsiloxane)-Based Microfluidic Devices," *Analytical Chemistry,* vol. 75, pp. 6544-6554, 2003.

[31] Y. Xia and G. Whitesides, "Soft Lithography," *Annual Review of Materials Science,* vol. 28, pp. 153-184, 1998.

[32] G. Lee, S. Chen and G. R. S. W. Huang, "Microfabricated plastic chips by hot embossing methods and their applications for DNA separation and detection," *Sensors and Actuators B: Chemical,* vol. 75, no. 1, pp. 142-148, 2001.

[33] I. John, Laser processing of engineering materials: principles, procedure and industrial application, Elsevier, 2005.

[34] D. Day and M. Gu, "Microchannel fabrication in PMMA based on localized heating by nanojoule high repetition rate femtosecond pulses," *Optics Express,* vol. 13, no. 16, pp. 5939-5946, 2005.

[35] R. Suriano, A. Kuznetsov, S. Eaton, R. Kiyan, G. Cerullo, R. Osellame, B. Chichkov, M. Levi and S. Turri, "Femtosecond laser ablation of polymeric substrates for the fabrication of microfluidic channels," *Applied Surface Science,* vol. 257, no. 14, pp. 6243-6250, 2011.

[36] C. Malek, "Laser processing for bio-microfluidics applications (part II)," *Analytical and bioanalytical chemistry,* vol. 385, no. 8, pp. 1362-1369, 2006.

[37] D. Snakenborg, H. Klank and J. Kutter, "Microstructure fabrication with a CO2 laser system," *Journal of Micromechanics and microengineering,* vol. 14, no. 2, p. 182, 2003.

[38] H. Klank, J. Kutter and O. Gescheke, "CO2-laser micromachining and back-end processing for rapid production of PMMA-based microfluidic systems," *Lab on a Chip,* vol. 2, pp. 242-246, 2002.

[39] J. Cheng, C. Wei, K. Hsu and T. Young, "Direct-write laser micromachining and universal surface modification of PMMA for device development," *Sensors and Actuators B: Chemical,* vol. 99, pp. 186-196, 2004.

[40] S. Wang, C. Lee and H. Chen, "Thermoplastic microchannel fabrication using carbon dioxide laser ablation," *Journal of Chromatography A,* vol. 1111, no. 2, pp. 252-257, 2006.

[41] C. Yang, K. Huang and J. Chang, "Manufacturing monodisperse chitosan microparticles containing ampicillin using a microchannel chip," *Biomedical Microdevices,* vol. 9, no. 2, pp. 253-259, 2007.

[42] H. Hou, Y. Wang, C. Chang, R. Yang and L. Fu, "Rapid glucose concentration detection utilizing disposable integrated microfluidic chip," *Microfluidics and nanofluidics,* vol. 11, no. 4, pp. 479-487, 2011.

[43] A. Tresansky, P. Joyce, J. Racide and J. Watkins, "Numerical Modeling of High-Energy Laser Effects in Polymer and Composite Materials," *Journal of Directed Energy,* vol. 5, pp. 137-158, 2014.

[44] M. Dustin and W. Roach, "A thermal model of laser absorption," in *Optical Interactions with Tissue and Cells XVII*, San Jose, California, 2007.

[45] P. Majumdar and H. Xia, "A Green's function model for the analysis of laser heating of materials," *Applied Mathematical Modelling,* vol. 31, pp. 1186-1200, 2007.

[46] F. Incropera, D. Dewitt, T. Bergman and A. Lavine, Principles of Heat and Mass Transfer, 7th ed., Hoboken, NJ: John Wukey, 2011.

[47] J. Shewchuk, "Unstructured Mesh Generation," in *CRC Handbook on Combinatorial Scientific Computing*, Boca Raton, FL, CRC Press, 2012, pp. 257-297.

[48] J. I. Leinhard and J. V. Leinhard, "Heat Transfer in Boiling and Other Phase-Change Configurations," in *A Heat Transfer Textbook*, Cambridge, MA, Phlogiston Press, 2001, pp. 437-499.

[49] M. James, Physical properties of polymers, New York: Springer, 2007.

Appendix

The curve fitting for the channel profiles was done using a curve fitting tool in MATLAB R2016A.

The fit is a gaussian curve with the following form:

$$f(x) = ae^{-(\frac{x-b}{c})^2} \tag{A.1}$$

The coefficient values for each of the cases are shown in table A.1.

Table A.1: Curve fitting values for considered laser beam radii

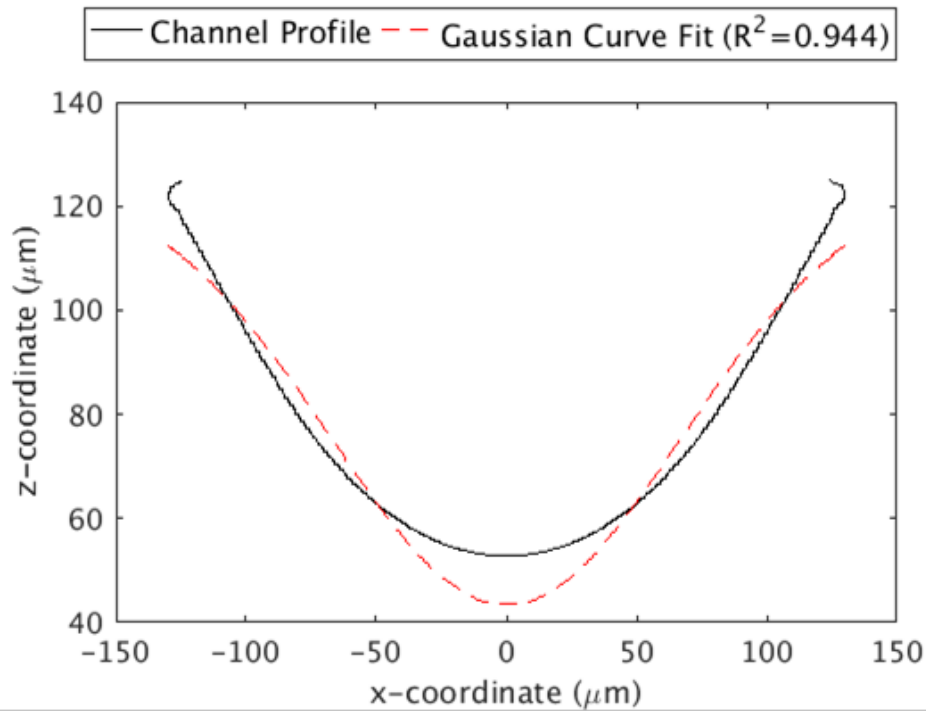|	92.5um	150um	300um	500um
a	43	36.294	24.7887	61.778
b	-0.0265	-0.0229	-0.0405	0.2434
c	88.0182	128.728	198.3528	630.7932
R-squared	0.97	0.9629	0.9286	0.7754

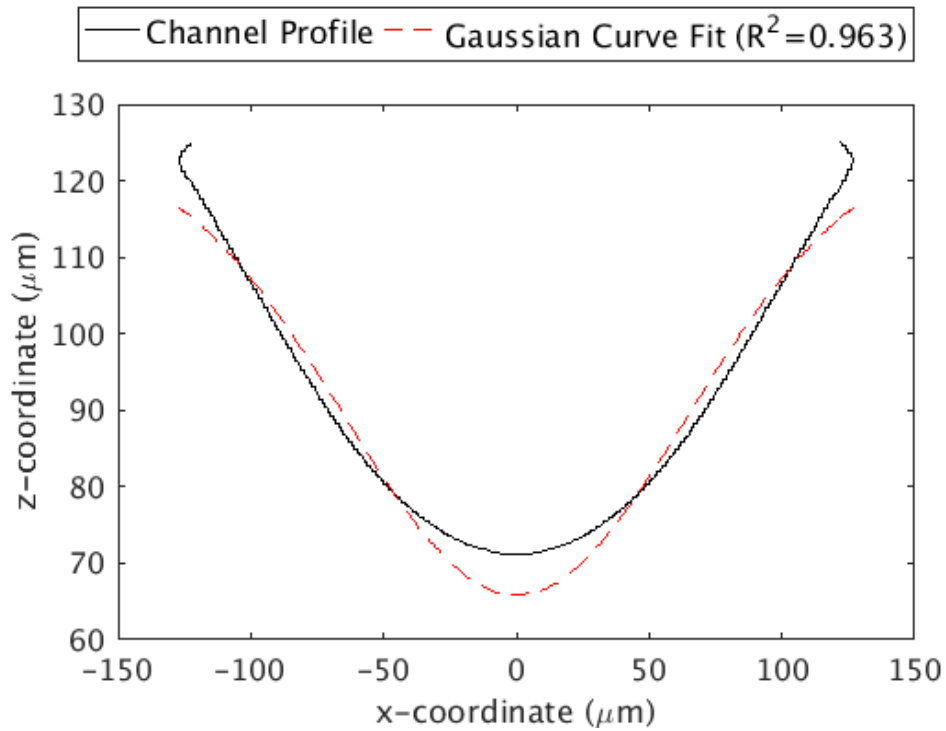Figure B.1: 100 mm/s channel profile with curve fit

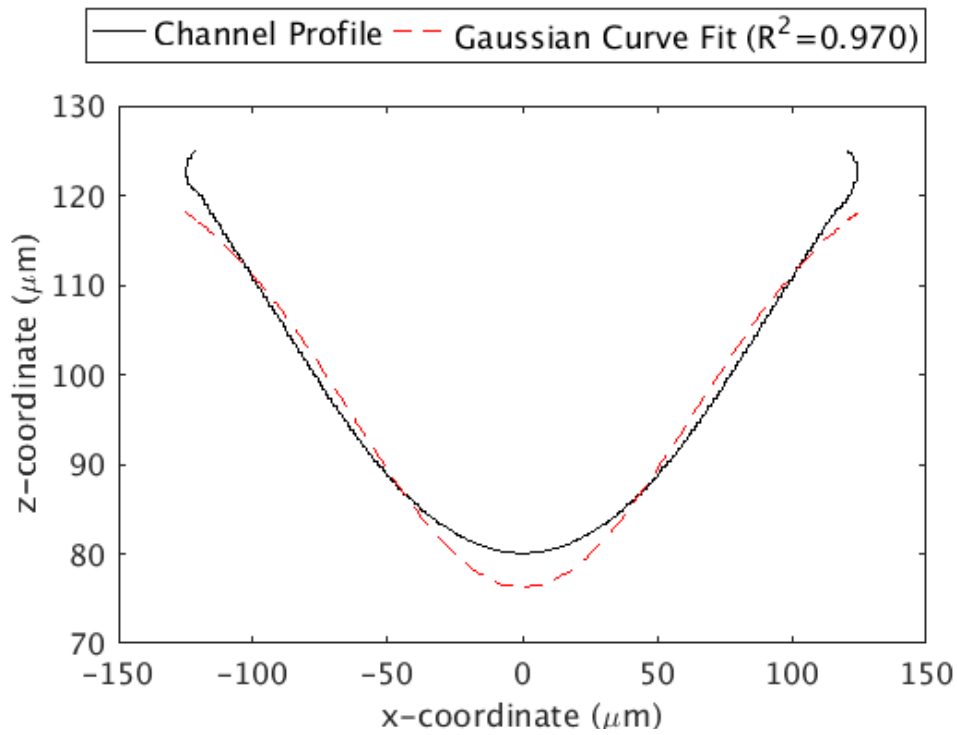Figure B.2: 200 mm/s channel profile with curve fit

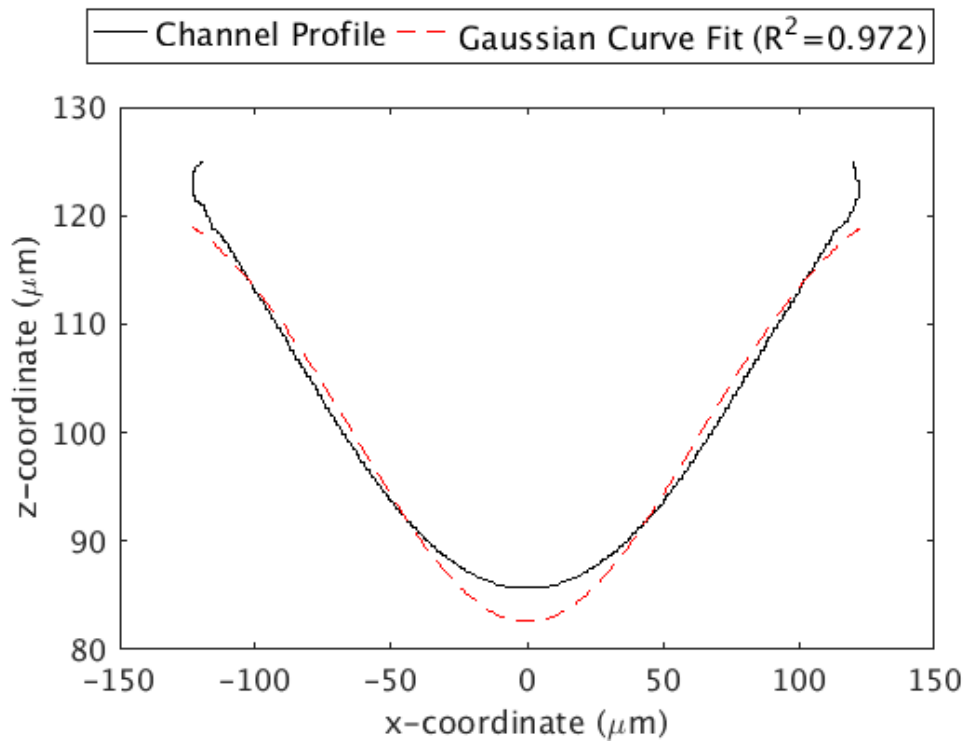Figure B.3: 300 mm/s channel profile with curve fit

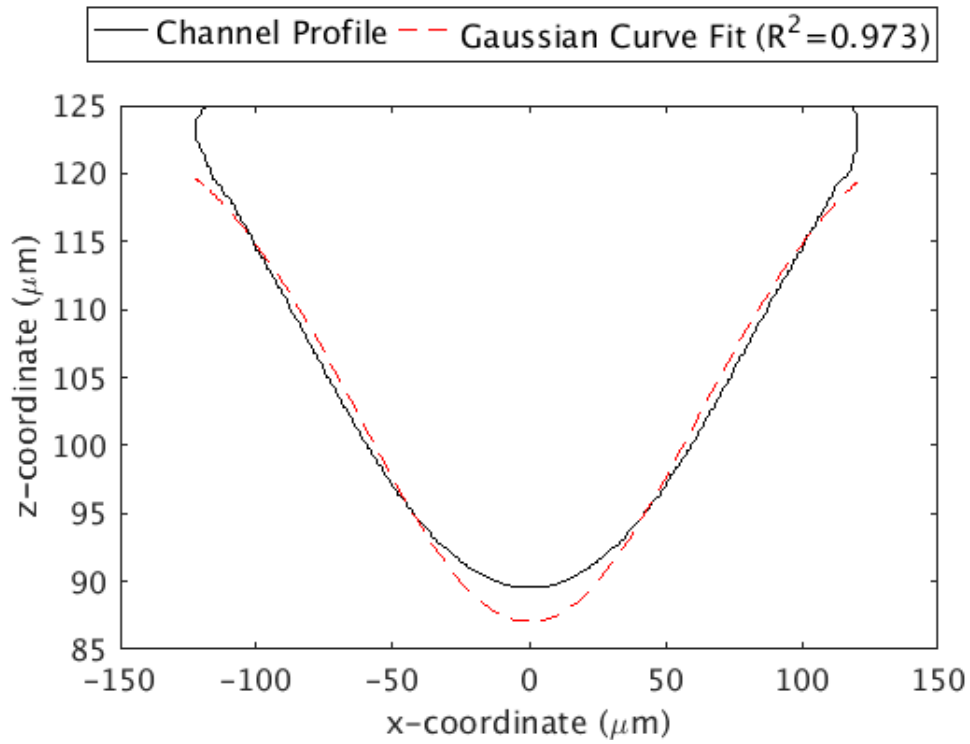Figure B.4: 400 mm/s channel profile with curve fit

Figure B.5: 500 mm/s channel profile with curve fit

Curve fitting was done using the same method has described for the laser beam radius. These

values are presented in table B.1.

Table B.1: Curve fitting values for considered laser scan speeds

	100um	200um	300um	400um	500um
a	81.6295	59.132	48.707	42.4619	38.0493
b	-0.0008	0.0095	0.013	-0.0003	-0.0328
c	95.2198	91.1305	98.3429	88.0139	87.1836
R-squared	0.9443	0.9628	0.9695	0.972	0.9732

Appendix C: Validation of simplification to 2D model

Actual depth values found, used to calculate the percent difference between 3D and 2D for validating using the 2D model over the 3D model.

Table C.1: 3D Convection Coefficient Depth Values

	h=10000	h=50000	h=100000	h=250000	h=500000
0.10	36	26	21	17	15
0.20	47	35	30	25	22
0.40	55	45	40	--	--
0.60	61	53	48	42	--

Table C.2: 2D Convection Coefficient Depth Values

	h=10000	h=50000	h=100000	h=250000	h=500000
0.10	38	26	21.0	17	15
0.20	49	36	30.5	25	22
0.40	57.5	48	42.0	35	31.5
0.60	62	55	50.0	43	39

Appendix D: Parametric Investigation of Thermal Conductivity

Higher values of thermal conductivity values considered, up to 5 Wm^{-1}K^{-1}.
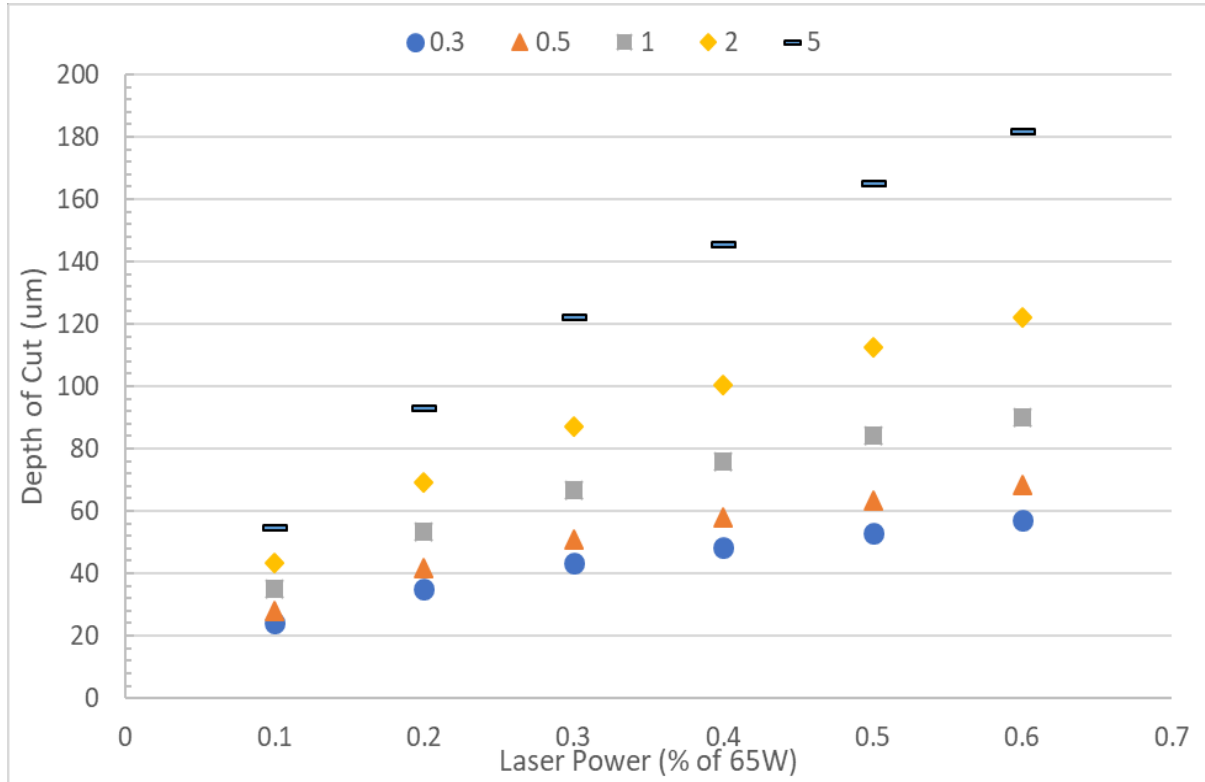

Figure D.1: Depth vs laser power for higher thermal conductivity values considered.